Materials Horizons

ROYAL SOCIETY OF CHEMISTRY

REVIEW

View Article Online
View Journal | View Issue

Cite this: *Mater. Horiz.*, 2023, **10**, 4827

Overview of the design of bionic fine hierarchical structures for fog collection

Danyan Zhan[a] and Zhiguang Guo *[ab]

Nature always uses its special wisdom to construct elegant and suitable schemes. Consequently, organisms in the flora and fauna are endowed with fine hierarchical structures (HS) to adapt to the harsh environment due to many years of evolution. Water is one of the most important resources; however, easy access to it is one the biggest challenges faced by human beings. In this case, fog collection (FC) is considered an efficient method to collect water, where bionic HS can be the bridge to efficiently facilitate the process of the FC. In this review, firstly, we discuss the basic principles of FC. Secondly, the role of HS in FC is analyzed in terms of the microstructure of typical examples of plants and animals. Simultaneously, the water-harvesting function of HS in a relatively new organism, fungal filament, is also presented. Thirdly, the HS design in each representative work is analyzed from a biomimetic perspective (single to multiple biomimetic approaches). The role of HS in FC, and then the FC performance of each work are analyzed in order of spatial dimension from a bionic perspective. Finally, the challenges at this stage and the outlook for the future are presented.

Received 13th July 2023,
Accepted 1st September 2023

DOI: 10.1039/d3mh01094e

rsc.li/materials-horizons

Wider impact

A novel perspective is proposed to analyze the design of fine hierarchical structures, which are vital for the efficiency of fog collection. In this review, an overall overview of recent work related to FC is given from a bionic perspective, and thus from a spatial dimensional perspective. This article thereby provides new inspiration for FC using HS inspired by nature and highlights how the design of the HS synergizes the three processes of fog water collection effectively.

1. Introduction

As is known, water is essential to human beings and creatures. Accordingly, satellite maps of the Earth appear almost totally blue because of its constitution of oceans. However, seawater cannot be directly used by organisms. Specifically, only freshwater can be utilized, which originates from rain, snow on mountains, underground water, *etc.* and makes up only 2.8% of the Earth.[1–4] Also, the freshwater distribution is unbalanced due to the variation in climate and geographic location. Presently, around two-thirds of the world's population has limited access to freshwater for at least one month of the year.[5] Furthermore, 500 million people face water scarcity throughout the year. According to the source of freshwater, researchers have devoted their efforts to alleviating this problem, as follows:[6–8] (1) construction of dams to collect precipitation, such as the Three Gorges Dam in China;[9] (2) digging wells to utilize underground water;[10] and (3) establishing methods to desalinate seawater.[11] However, the above-mentioned approaches often require significant labor and economic costs. Also, the regions that are affected by a lack of water resources are both developing and even relatively undeveloped, for instance, the coastal deserts of West Africa (Namibia), South America, the Middle East.[12] Evidently, these methods cannot resolve all the problems of dehydrated regions. Also, besides climate dramatic change, water wastage, water contamination, and others are causing the amount of available freshwater to decrease.[13–15] This has resulted in vast challenges in making freshwater available in inherent arid regions on Earth. Furthermore, the World Economic Forum listed that the water crisis will become the biggest latent effect of global risk by 2025.[16] Thus, it is urgent to develop novel methods to produce portable freshwater in arid and semi-arid areas.

In fact, the source of fresh water is not only precipitation but also atmospheric water. During the natural ecological circulation, precipitation eventually becomes atmospheric water. Atmospheric

[a] *Ministry of Education Key Laboratory for the Green Preparation and Application of Functional Materials, Hubei University, Wuhan 430062, People's Republic of China. E-mail: zguo@licp.cas.cn; Fax: +86-931-8277088; Tel: +86-931-4968105*

[b] *State Key Laboratory of Solid Lubrication, Lanzhou Institute of Chemical Physics, Chinese Academy of Sciences, Lanzhou 730000, People's Republic of China*

water is a ubiquitous clean water resource, where the atmosphere contains approximately 1.29×10^{16} kg of water in total.[17] Frequently, humans admire the ability of creatures to survive in harsh environments. This has also caused humans to be interested in comprehensively understanding how these creatures live and by what mechanisms, especially in the arid desert. In early 1727, Hales reported one of the earliest studies on plants absorbing atmospheric water. In 2014, Malik *et al.* reviewed the direct absorption of water from the atmosphere by plants and animals, providing an alternative approach to addressing the freshwater crisis.[18] To date, researchers have developed many projects related to atmospheric water collection (AWC). AWC can roughly be divided into three types, *i.e.*, artificial rain collection,[19] dew water collection,[20] and fog collecting (FC).[21,22] Artificial rain collection is affected by the environment and can only be realized under tropospheric conditions where clouds gather.[23,24] Dew collection is minimally impacted by weather conditions and geographic location in comparison to artificial rain collection and FC.[25,26] Consequently, dew collection is widely acknowledged as a superior approach to freshwater collection. Nonetheless, there are technical challenges involved in dew water collection, which must be resolved, such as the absence of cost-effective radiators to optimize the yield of water and the necessity of tailoring materials to the location and the particular climatic conditions.[5] In recent years, fog collectors have gradually developed and their efficiency of water collection improved.[27] In terms of collection efficiency, operating cost, overall flexibility, and other factors in comparison to the two other types, FC exhibits the characteristics of simple and continuous technology with low-cost technical requirements.[28]

However, although FC is appropriate for arid and semi-arid areas, some major challenges still exist, as follows: (1) typically, relatively high humidity environmental conditions are required for FC and (2) poor collection efficiency.[29,30] In recent years, researchers have found that specific MOF materials can achieve considerable water absorption in a limited range of relative humidity.[31–33] This introduces novel opportunities for AWC. Therefore, developing new composite materials with effective adsorption–desorption droplet cycling capabilities is a significant concern in the AWC sector. Numerous studies have analyzed this topic extensively. Thus, the present review is focused on enhancing the collection capacity of conventional FCs under specific saturated relative humidity conditions from a novel perspective.

Following the laws of nature, researchers ingeniously simulated the structure of organisms to collect fog. It can be found that the combination of FC with bionics can improve the efficiency of FC.[34] Taking *Cotula fallax* leaves as an example, they possess a special three-dimensional HS, consisting of fine hairs covering the leaves. These HS can perform asymmetric anisotropic fog collection. In addition, the fine hairs can ensure effective fog collecting.[35] Besides *Cotula fallax* leaves, the structure of cactus has three parts based on scanning electron microscopy (SEM) observation,[36] including barbs with tips, facilitating the capture of small droplets in the air, and ridges with gradient grooves. Among them, the grooves possess a hierarchical structure. This HS that can quickly transport droplets to improve the efficiency of FC. However, FC is divided into three parts, including capturing and coalescing the fog, transporting the coalesced droplets, and storing the rolling water drops.[17] Thus, it is not enough to simulate the HS because simulating a single HS of a certain creature only improves one process of FC. Accordingly, significant research is devoted to successfully completing materials with HS to improve the efficiency of FC. In this case, bionic materials with HS may significantly improve the laboratory efficiency, but there are some issues that need to be urgently resolved in the actual situation. Firstly, the improvement in efficiency one the laboratory scale may be a million to one for the real situation.[37] Secondly, is it possible that the collected drop waters will be evaporated by solar collectors. Finally, none of the reported materials are suitable for commercial applications.

In this review, we systematically discuss the recent ingenious designs of HS materials inspired by organisms and the strategies for improving the efficiency of FC. Firstly, the fundamental principles of FC are discussed. Secondly, the role of HS in fog collection is analyzed in terms of the microstructure of typical examples of plants and animals. Additionally, the fog-harvesting function of HS in a relatively new organism, fungal filaments, is presented. Thirdly, the design of HS in each representative work is analyzed from a biomimetic perspective, ranging from single to multiple biomimetic approaches. The function of HS (HS design in fog collectors with varying spatial dimensions) in FC and the FC efficiency of each work are investigated in sequence according to spatial dimension, from a bionic viewpoint. Finally, the obstacles encountered at this stage and future prospects are discussed.

2. The mechanisms of fog collection with HS materials

2.1 Fog capture and coalesce

Once impacted by fog flow, HS materials will collide with fog droplets, causing the gradual condensation of small water drops. The aggregated droplets will roll along established tracks into collectors until the size of the small droplets grows enough to overcome gravity.[16] Obviously, the whole fog collection process using HS materials involves main two processes, *i.e.*, capturing and coalescing the fog and transporting the coalesced droplets. Thus, to provide readers with a theoretical understanding of the fog collection process, the internal mechanisms of these two processes will be introduced in detail in the following section.

2.1.1 Young's equation and contact angle. Wetting refers to a gas, liquid, and solid three-phase interface. Supposing a drop of liquid is placed on an ideal solid surface to form the shape shown in Fig. 1a, the angle at the three-phase interface from the solid–liquid to the gas–liquid interface is called the contact angle, θ. The three-phase interfacial tension generally obeys Young's equation, as follows:[38]

$$\gamma_{SG} = \gamma_{SL} + \gamma_{LG}\cos\theta \quad (2.1)$$

where γ_{SG} represents the solid-gas interfacial intention; γ_{SL} represents the solid–liquid interfacial intention; and γ_{LG} represents the

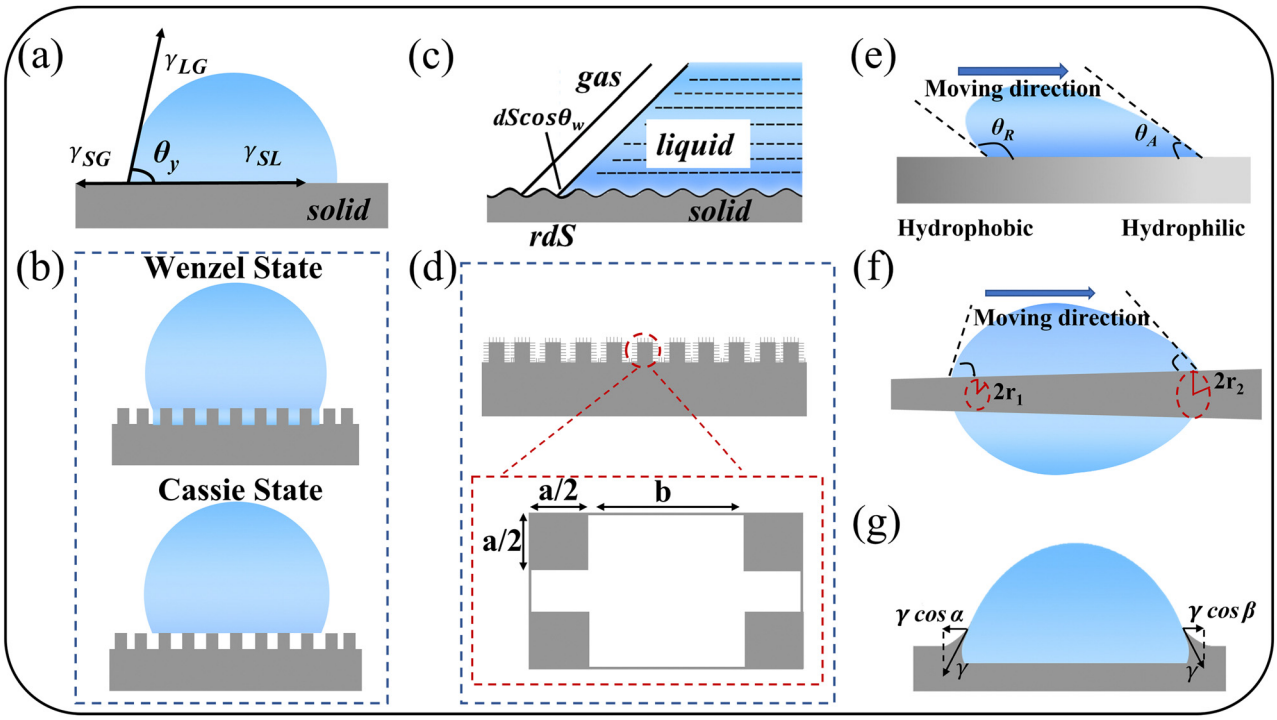

Fig. 1 (a) Contact angle of a droplet at equilibrium on an ideal solid surface. (b) Possible state of a droplet on a rough surface (compound wetting state: between CB state and Wenzel state). (c) Influence of surface roughness on the CA. (d) Model of roughness geometry for theoretical analysis. (e) Water transport behaviour on a patterned surface. (f) Water transport behaviour on a conical spine. (g) Directionally pumping droplets by capillary force on a slippery surface with oil meniscus.

gas–liquid interfacial intention. Young's equation is the basis for the research on solid–liquid infiltration. In general, to characterize the wettability of a material surface, the liquid contact angle (CA) of the solid surface must be used. When θ is less than 90°, the liquid can wet a certain area of the solid surface; when θ is between 90° and 150°, the solid surface is hydrophobic; and when the θ is greater than 150°, the surface is superhydrophobic (SHB).

2.1.2 Wenzel and Cassie Baxter theory. According to the description above, Young's equation describes the wettability on an ideal surface but starts to fail when it is applied to the real situation of a rough surface, as shown in Fig. 1b. Thus, in 1936, Wenzel[39] introduced the concept of surface roughness in the theory of wetting behaviours and obtained a modified Young's equation based on comprehensive consideration of the effect of roughness on wettability. The true area of a rough surface is not the same as the apparent surface area, and the ratio of the true surface area to the apparent surface area is defined as the surface roughness. When the droplet interface advances, the apparent surface area of the liquid interface increases by dS, and the true area of the solid–liquid surface increases by rdS. Thus, the true area of its interface decreases by rdS, and the true area of the liquid–gas interface (apparent area) increases by d$S\cos\theta_w$, as shown in Fig. 1c. In the equilibrium state:

$$\gamma_{SL} r\mathrm{d}S - \gamma_{LG}\mathrm{d}S\cos\theta_w + \gamma_{SG}\cos\theta = 0$$
$$\cos\theta_w = \frac{r(\gamma_{SG} - \gamma_{SL})}{\gamma_{LG}} = r\cos\theta_y \quad (2.2)$$

where is θ_y represents Young's contact angle.

The surface morphology of real solids is very complex. In 1944, considering the importance of surface chemistry, Cassie–Baxter further provided a more complex model by introducing new coefficients in the above-mentioned equation.[40] Also, considering the influence of different chemical factors on wettability, they proposed a combined model of surface morphology and chemical properties of several different materials and described them by "n". In addition, "n" for different types of materials is randomly distributed. Each material has a specific surface tension, *i.e.*, $\gamma_{i,SL}$ and $\gamma_{i,SA}$ on the surface with area fraction f_i, satisfying the following equation:

$$f_1 + f_2 + \ldots + f_n = 1, \quad \gamma_{SA} = \sum_i^n f_i(\gamma_{i,SA}), \gamma_{SL} = \sum_i^n f_i(\gamma_{i,SL})$$
$$\cos\theta_{CB} = \sum_i^n f_i(\gamma_{i,SA} - \gamma_{i,SL}) \Big/ \gamma_{LA} = \sum_i^n f_i\cos\theta_i \quad (2.3)$$

Analysing a simplified case where the composite surface is composed of two different materials, after applying the CB equation, the apparent contact angle of the material surface can be extrapolated to the following equation:

$$\cos\theta_{CB} = f_1\cos\theta_1 + f_2\cos\theta_2 \quad (2.4)$$

For a composite interface consisting of a solid–liquid part and a liquid–air part, as shown in Fig. 1d, the air will be trapped in the cavity formed by the rough structure, making the droplets

lie on the surfaces of both the solid and the air cavity, corresponding to the free integral numbers f_{SL} and f_{LA} (f_{SL} + f_{LA} = 1). Combining the roughness coefficient r and the CB equation, as well as the contact angle of the liquid on the solid and the air, the following equation, can be deduced:

$$\cos\theta_{CB} = rf_{SL}\cos\theta_0 + f_{SL} - 1 \quad (2.5)$$

When f_{SL} = 1, the CB equation can be transformed into the Wenzel equation. The CB equation can be transformed as follows:

$$\cos\theta_{CB} = 1 + f_{SL}(\cos\theta_0 - 1) \quad (2.6)$$

where f_{SL} represents the proportional fraction of the solid–liquid phase in the contact area on the rough surface. This is different from the Wenzel state. Because the rough structure must be filled with liquid before the droplets reach it, this is the so-called "impregnated" CB wetting state.[41] Based on the CB equation, it is possible to produce a rough structure on the surface and control the surface morphology to bring the solid fraction f_{SL} close to zero. When θ_{CB} is less than 90°, the smooth and flat substrate is inherently hydrophilic, and θ_{CB} can change from hydrophilic to hydrophobic as r increases. Compared to the Wenzel model, this model has better applicability. The CB equation considers both the surface chemical composition and surface and accurately determines the wetting state of the material surface.

2.1.3 Hierarchical structure model. The surface of HS materials is not a single-scale surface structure, often possessing two or more levels of graded structures, such as the large micron protrusions and small nano protrusions on the surface of lotus leaves. In this case, neither the Wenzel nor Cassie–Baxter equations can well explain the wetting state on the surface of the HS. However, an HS structure model can be developed based on them. Patankar *et al.*[42] emphasized the importance of the multiscale roughness affecting the surface of the lotus leaf and theoretically modeled the effect of the surface geometry of the lotus leaf structure on its surface properties. Based on the Wenzel and CB equations, they proposed a model with a hierarchical structure. The model has a secondary combinatorial array of manometer-sized square columns of uniform size and shapes with side lengths a_1 and a_2. In this model (Fig. 1d), the geometry of square columns on two scales is assumed to be periodic, the cross-sectional dimensions of the columns are $a \times a$, and their spacing is b. In this model, the solid roughness f_{SL} is shown as follows:

$$f_{SL} = A_1 = \frac{1}{[(b_1/a_1) + 1]^2} \quad (2.7)$$

wherein, the subscript 1 here expresses that a_1 is a kind of geometric parameter.

Based on this, the modified CB equation is derived as follows:

$$\cos\theta_{CB} = A_1(1 + \cos\theta) - 1 \quad (2.8)$$

where H_1 is the height of the micrometer column. It is clear from the above-mentioned equation that increasing the ratio of column height to column spacing (H_1/a_1) favours hydrophobicity.

2.2 Droplet transport

The captured droplets gradually grow, and then gradually polymerize with adjacent small droplets to form large droplets, releasing binding energy.[20,43] The dynamic behaviour of the droplet transport removal process varies, and the revelated basic theory of droplet transport is discussed below.

2.2.1 Wettability gradient-driven surface. The design of subtle HS is commonly seen in patterned surface structures (hydrophilic–hydrophobic alternation), the application of Janus films,[44] *etc.* (discussed in detail in Chapter 4). On a surface with gradient wettability, water droplets move toward more hydrophilic regions in the absence of external forces. The driving force generated by the surface energy gradient can be calculated using the following equation:[45,46]

$$F_{wet} = \int_{L_f}^{L_t} \gamma(\cos\theta_A - \cos\theta_R)\mathrm{d}l \quad (2.9)$$

where γ, θ_A and θ_R represent the surface tension, forward CA, and backward CA of water, respectively. Also, dl stands for an integral variable along the length of the SHB region (L_f) to the superhydrophilic (SHL) region (L_t). According to eqn (2.9), water droplets are spontaneously transported directionally from the SHB region to the SHL region, driven by a surface gradient (Fig. 1e). Similarly, the movement of water droplets toward the hydrophilic zone can be observed on Janus materials with opposite wettability on both sides.[16]

2.2.2 Laplace pressure gradient-driven surface. Conical needle-like structures with significantly different radii at both ends are common on cactus and spider silk. Needle-like materials often possess HS (detailed discussion in Chapter 3). Droplets spontaneously move from the side with the smaller radius to the side with the larger radius (Fig. 1f).[47] This phenomenon can be attributed to the Laplace pressure gradient of the conical spines, as follows:

$$\Delta P = \int_{r_1}^{r_2} \frac{2\gamma}{(r + R_0)^2}\sin\beta\mathrm{d}z \quad (2.10)$$

where r represents the local radius (r_1 and r_2 are the local radii of the conical spines on either side of the droplet). Also, R_0, which is equal to $\left(\frac{3V}{4\pi}\right)^{\frac{1}{3}}$ (V is the volume of the droplet), represents the droplet radius. β is the half-top angle of the conical spine and z is the integral variable along the diameter of the conical spine. The Laplace pressure on the high-curvature side of the conical spine has a greater effect on the droplet than on the two-curvature side, driving the droplet to the high-curvature side.

2.2.3 Capillary-driven surface. Inspired by the extraordinary ability of organisms to collect fog, the above-mentioned strategies of droplet transportation are driven by the surface wettability gradient and Laplace pressuredifference.[48–51] However, at the onset of mist collection, the nucleated droplets are too small to efficiently move under this actuation transport. This is because at tiny scales, the contact angle hysteresis becomes the dominant factor, while the external driving force

becomes insignificant.[52] It is worth mentioning that nature has ingenious ways of transporting small volumes across liquid surfaces.[53] In the case of a liquid irrigation surface with an oil meniscus, it is a small droplet that can be pumped quickly and directionally around the oil meniscus when the mist is collected. The reason for this is that one side of the droplet overlaps with the oil meniscus and rises. Here, there is a difference between contact angles α and β on both sides of the droplet (Fig. 1g). The driving force is also low, and the capillary attraction force is understood as follows:[54–56]

$$F_c = \gamma R(\cos\alpha - \cos\beta) > 0 \quad (2.11)$$

where α (°) and β (°) are the contact angles of the left and right sides of the droplet, respectively, and γ (mN m^{-1}) is the oil/gas interfacial tension. R (mm) is the radius of the droplet. The force is mutual. There is also resistance while being driven, as shown by the following equation:

$$F_d \sim \eta RU \quad (2.12)$$

$$U \sim \gamma/\eta(\cos\alpha - \cos\beta) \quad (2.13)$$

where U (m s^{-1}) is the moving speed and η (mN s m^{-2}) is the viscosity of the filling lubricant. The maximum moving distance of the droplet is determined by the length of the oil meniscus. Simultaneously, the effective capillary length is produced by the oil meniscus, as shown in the following equation:

$$\lambda = (\gamma/\rho g)^{1/2} \quad (2.14)$$

where ρ (g cm^{-3}) is the moving speed of the droplet and g is the acceleration due to gravity. Therefore, in the effective capillary length range, droplet pumping behaviour without external energy input can be achieved under the capillary force generated by the oil meniscus.

The above-mentioned theoretical basis for the three processes related to fog water collection can help researchers understand the specific wettability of typical plant and animal surfaces. This makes it possible to clearly analyse the factors influencing the fog collection efficiency. Subsequently, the design of the corresponding grading structure can be used to improve the efficiency of fog collection by considering the relevant factors. The following are examples of the specific wettability of the most common plants and animals found in nature.

3. The functions of hierarchical structures in organisms

3.1 Botanical category

Creatures are worthy to be studied by human beings. They have evolved for several hundred million years to adapt to the harsh environment. Scientists perceive that some organisms show a degree of special wettability by relying on the HS. HS is are composite structures, containing micro- and nano-bilayer structures, or microstructures formed by sub-microstructures and others.[57] In this case, taking advantage of the functions of HS in organisms may cleverly synergize the two processes of FC to efficiently store water.[58–60] Thus, first understanding the functions of HS in organisms is important. In this part, we analyze the role played by HS in the special wettability of typical plants, animals, and microorganisms.

3.1.1 Lotus leaves. In the summer, lotus flowers are common plants. In ancient China, they were hailed by the literati as a symbol of cleanliness, because they had the characteristic of being undefiled by mud, which is presently known as the ''lotus effect''. This special character attracted interest from researchers. In 1997, German scientist Barthlot first revealed the mystery of the lotus effect, which is attributed to the micron-scale mastoid and waxy surface layer of lotus plants.[61] In 2002, Jiang *et al.*[57] discovered that there is a mass of nano-scale granule structures on each micron-scale mastoid, namely, micro-nanostructures, through field-emission scanning microscopy (FE-SEM). As shown in Fig. 2a$_3$, there are uniformly distributed structures with a size of 5–9 μm on the surface of the lotus leaf. Meanwhile, as can be seen in Fig. 2a$_4$, rod-like structures with a size of 50–70 nm are distributed uniformly on the secondary surface of the lotus leaf.[62] These structures prevent droplets from entering the space in the surface of the lotus, that greatly reducing the contact area between the water and the surface. Simultaneously, they also reduce the adhesion between a solid and liquid. Guo *et al.*[62] certified the surface of the lotus has the characteristic of superhydrophobicity by measuring the static CA (around 162°) and sliding CA (around 3°) (Fig. 2a$_1$ and a$_2$, respectively). Therefore, the HS (micro nanostructure) is responsible for the superhydrophobicity of the surface of lotus leaves, without considering their surface chemistry. This can inspire the design of structures for the transportation of droplets during FC. Surprisingly, the wettability of the back surface of the lotus leaf is vastly different from the surface exposed to the air. Cheng *et al.*[63] found that the back surface of the lotus leaf possesses normal hydrophilicity. It is constituted of many flat plates and mastoids. Each mastoid is covered with nanoscale groove structures. Besides, it may present hydrophilic substances.[65] It is clear the HS and hydrophilic substances lead to hydrophilicity. HS combine different properties of chemical substances, causing the superhydrophobic surface to transform into superhydrophilic.

The HS constructs the roughness. As the roughness increases, the hydrophilic surface becomes more hydrophilic, while the hydrophobic surface becomes more hydrophobic.[66] Super- hydrophilicity is vital for capturing fog.[67] However, transporting water droplets requires the material to have superhydrophobicity.

3.1.2 Taro leaves. The Lotus leaf is researched the most. However, taro (*Colocasia esculenta*) is the fourth most consumed crop globally.[68] The characteristic hydrophobicity of taro leaves has also received great attention. The basic structure in the surface of the taro leaf consists of microscale elliptical bumps with a diameter of around 10–30 μm,[69] which are covered by nanoscale structures, *i.e.*, waxy nanoscale epicuticular crystals, as shown in Fig. 2b$_3$ and b$_4$. The formation of HS is attributed to the harmonious dissemination of many nanoscale structures, resulting in the formation of a microstructure. The HS is similar to the above-mentioned lotus leaf. The difference is that the microscale bumps and second surface of the taro leaf distribute

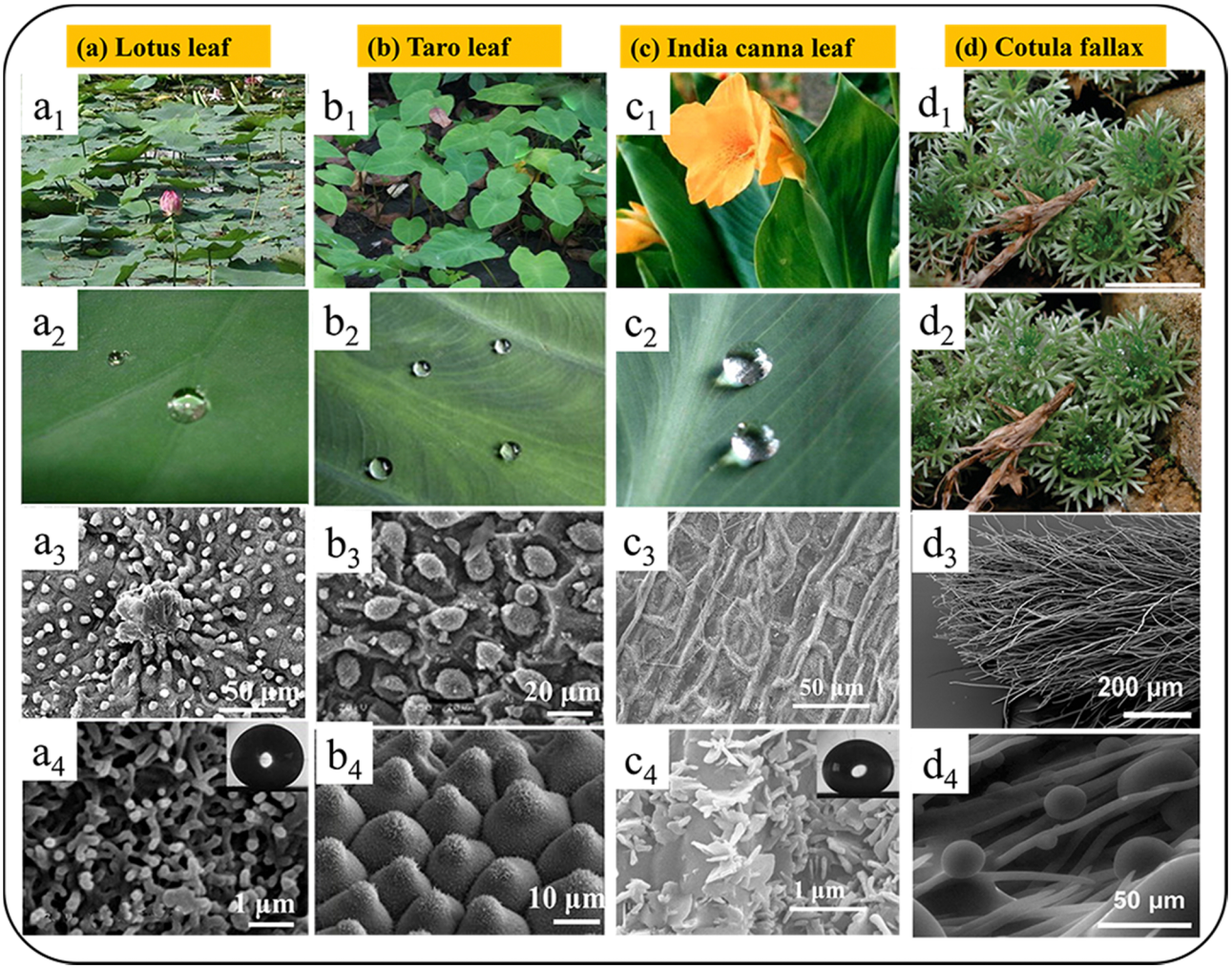

Fig. 2 Example of botanic surfaces with special wettability and surface topography. (a) Lotus leaf. Digital photos and SEM image.[62] (Copyright: 2007, Elsevier.) (b) Taro leaf. Digital image.[64] (Copyright: 2020, Nature) and water state on the surface and SEM images.[69] (Copyright: 2011, Elsevier) (c) India canna leaves. Photos of a few water droplets floating on an India canna leaf and SEM images.[62] (Copyright: 2007, Elsevier.) (d) *Cotula fallax*. Dry plant, water on the surface, and SEM micrographs of Cotula flax.[35] (Copyright: 2011, the American Chemical Society.)

the average nanoscale needle structure (diameter of 20–50 nm).[62] The presence of these bumps can increase the CA (90°–150°) of the surface, making it superhydrophobic in nature.[70] The water collected by taro leaves can be absorbed by the root of the plant after tumbling into its root. The nanostructure has the effect of increasing the roughness of the surface to the air between the atmospheric water and the leaves. This is why taro leaves exhibit superhydrophobicity (Cassie–Baxter theory). Different nanostructure shapes may affect the efficiency of collecting atmospheric water. It is the magic of nature that makes various microcosmic plant leaves use atmospheric water in different ways. This brings another type of inspiration in designing materials with nanoscale patterns to collect fog.

3.1.3 Other botanical leaves. In the previous sections, we carefully analysed the HS of the lotus leaf and taro leaf as examples. However, in nature, there are many other superhydrophobicity plant leaves with similar microscopic HS. The SEM image (Fig. 2c_1–c_4) of the surface of a canna leaf shows a random distribution of microscale bumps, which consist of sub-microscale rod-like structures (diameter of 200–400 nm).[62] Also, clover, which is considered to be a symbol of luck, is superhydrophobic. Water droplets appear spherical on the surface of clover. Its microstructure is a map-like microscale structure, consisting of a nanoscale needle structure present on the microcosmic surface.[71] In the case of both the canna leaf and clover, their static CA is greater than 160°,[72] exhibiting the characteristic of superhydrophobicity. However, they only can capture fog and do not show the ability to collect water. *Cotula fallax* has the remarkable ability to collect water. *Cotula fallax* leaf also has complicated HS (Fig. 2d_1–d_4). Each leaf is covered with hairs that have two different lengths (long hairs of 2–5 mm and short hairs of less than 500 μm[35]). These two types of hairs have fine nanostructures with well-defined ridges, which along run the length of individual hairs, stretching from close to the tip to just short of the hair root. Also, longitudinal grooves are present around the entire circumference of each hair. Because the individual leaves of *Cotula* fallax are very

close, the longer hairs of adjacent leaves can overlap and intertwine to form a "cushion" structure, efficiently offering a network structure to support droplets.

3.1.4 Nepenthes alata. It is not difficult to find that the above-mentioned botanical leaves have the same characteristic of superhydrophobicity. When they contact the air, the atmospheric water can form spherical droplets on their surface. However, the droplets cannot move directionally. Some plants have the property of directional movement of water droplets. This behaviour is usually ascribed to HS.[46,49] The typical plant is *Nepenthes alata*. The surface of its multiscale peristome margin has the phenomenon of continuously and directionally transporting water droplets. Its superior margin is an arched ring of tissue, which is called the bottle lip. Chen *et al.*[73] observed the flow of droplets on the surface of the bottle lip with a high-speed camera. They discovered that directional transport occurs from the inside to outside, where the droplets can shift from the inside edge of the bottle lip to the outside within seconds, while those on the outside of the bottle lip cannot move into the inside. According to the high-resolution images (Fig. 3a–d), water transportation is only limited in the distribution of approximately ten microchannels in the large channel. The microchannel consists of an arched microcavity. These structures may lead to the directional movement of water. The microcavity has subtle HS, which are regular radium ridges arranged in a microcavity. During the process of FC, directional transportation can benefit the concentration of water in a certain container and reduce the water loss caused by external factors. Thus, based on the above-mentioned superhydrophobic leaves, *Nepenthes alata* brings new inspiration for directional transportation.

3.1.5 Cactus. There is no mention of the capacity of FC for the above-mentioned plants. Nevertheless, their special wettability can be designed in a certain process of FC. When referring to plants for FC, the most admired plant is the cactus. In the desert, cactus can tenaciously survive regardless if the weather is extremely hot.[74] Therefore, it is interesting to wonder how it collects water to meet its demand. The first impression of cactus is that it has spines, which are distinct from other plants. Based on the research by many scientists regarding how it collects water, is has been found that its spines with HS ensure its fundamental life in extremely harsh external environments, such as highly arid deserts.[75] Ju *et al.*[36] investigated the microstructure of the spines of cactus in detail. The SEM image (Fig. 3f) showed the presence of three parts in the microstructure of the spines, as follows: (1) the tip contains oriented bards, (2) the middle contains gradient grooves, and (3) the base contains belt-structured trichomes. Further, the magnified images of the middle portion of the spine revealed multi-level grooves, *i.e.*, HS (Fig. 3g–j). The HS contains microgrooves and sub-microgrooves. Yi *et al.*[76] revealed the behaviour of droplets on the spines. At the tip of the conical spine, small droplets are captured and deposited. The size of small droplets can increase gradually until the adjacent droplets merge. Finally, they can form a bigger drop. The bigger drops are spontaneously transported from the tip to the base of the conical spine, which is driven by the Laplace pressure difference generated by the shape of the conical spine. The HS of the spine can accelerate the formation of bigger drops.

3.2 Animal category and microorganisms

3.2.1 Desert beetle. In the world, a hyper-arid region is the Namibian coast, where rainfall is scarce.[77] In the Namib desert, its environment is extremely harsh, such as a great temperature difference between daytime and night and heavy fog in the morning. The fauna and flora living here survive by using fog precipitation as their source water.[78] The Namibian desert beetle is the subject of widespread interest regarding how it obtains water. In an early report, it was shown that it obtains fog by simply exposing its back to the direction of fog flow directly.[79] The HS on its back is not like that of plants whose HS are micron-nanostructures. Parker *et al.*[58] uncovered that there are wax-coated hydrophobic areas and hydrophilic wax-free parts randomly distributed on its bumpy surface (Fig. 4a–c). The beetle makes use of the contact between its back and the fog. The water vapor accumulates on its back due to the alternating hydrophobic and hydrophilic parts on its back. From a micro perspective, firstly, the fog vapor deposed on the hydrophilic peaks forms fast-growing droplets. Secondly, the size of the droplets can grow too large to be static. Finally, the droplets can overcome gravity to roll off the hydrophilic surface and roll along the hydrophobic area until they roll into the mouth of the beetle, which is induced by the surface wetting gradient. Accordingly, designing functional HS inspired by the desert beetle, namely, superhydrophobic/superhydrophobic materials, is a good way to achieve FC. This may avoid the requirements of expensive materials and large instruments.

3.2.2 Spider silk. The spider is another insect with the ability to collect water from the air.[80] It is different from the desert beetle, which collects fog by exposing its back to the direction of fog flow. Spiders can hunt for food by using their own silk to form a spider web. Actually, the source of water for a spider is the condensed water on its spider web.[81] The compounds in spider silk are humidity-sensitive hydrophilic flagelliform proteins.[82,83] In 2006, Emile *et al.*[84] revealed the structure of spider silk, which is characterized by periodic spindle knots and joint. The knots are composed of nanofibrils, favouring the condensation of water drops, spaced along two main-axis fibres. Thus, the HS in spider silk are its spindle knots and joints. In 2010, Zheng *et al.* depicted that spider webs are built by cribellate spiders using a cribellum, which is a comb-like device, to separate the silk fibres and revealed why the spider silk can collect water from fog, as shown in detail in Fig. 4d and e.[83] The HS, *i.e.*, the spindle knots and joints, can lead to a surface energy gradient and Laplace pressure difference. Exposing desiccated spider silk to fog, its structure can change as water starts to form droplets, which is driven by wettability. Initially, the knots are semi-transparent puffs. As the droplets continuously condense on the puffs due to the hydrophilic nanofibrils, the puffs can transform into opaque bumps until they form periodic spindle knots. Once the HS of periodic spindle knots and joints are formed, directional transportation is induced by

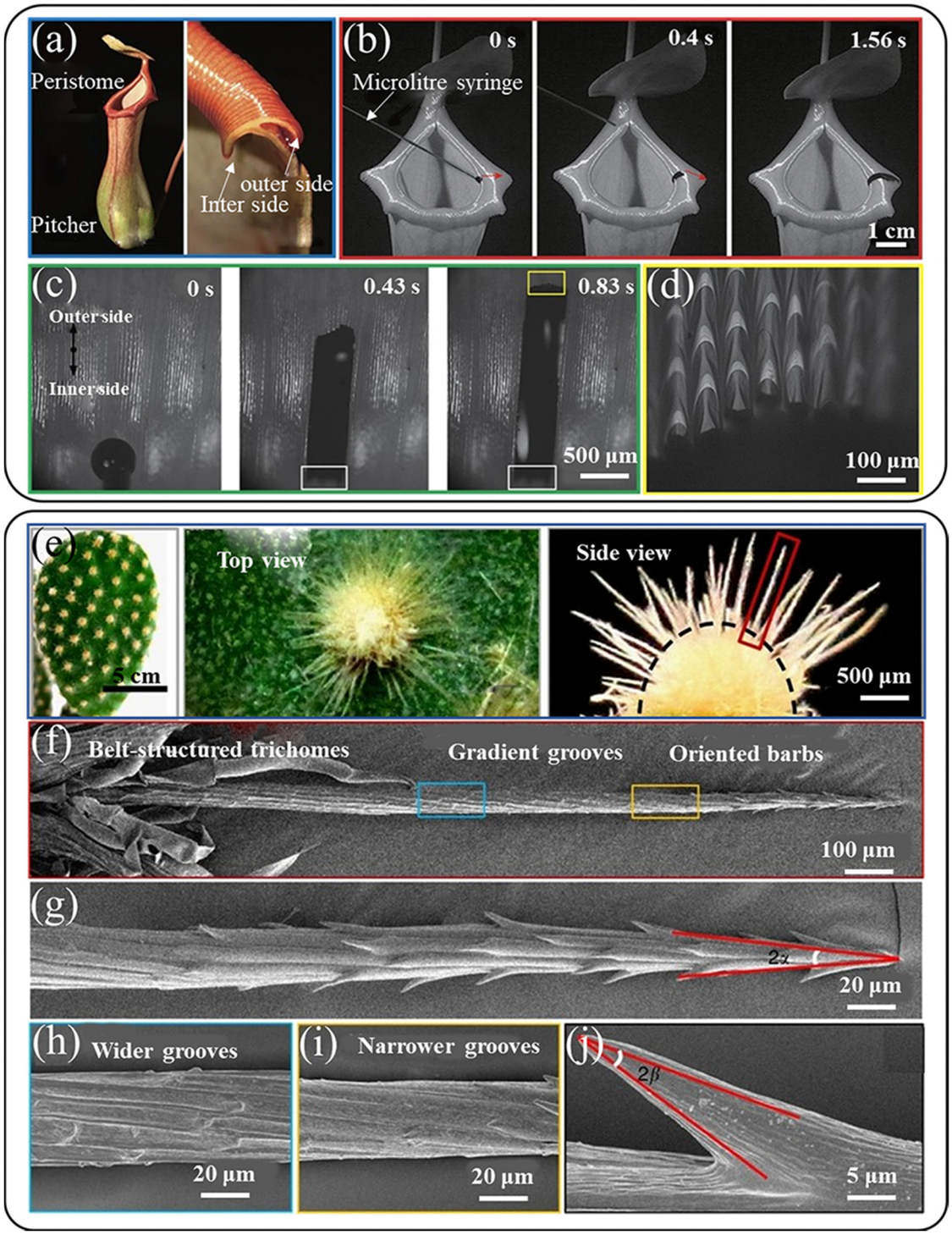

Fig. 3 Digital photos of (a) *Nepenthes alata* and (b) water transport behaviour in its peristome and (c) and (d) a single large channel. Reproduced with permission.[73] (Copyright: 2016, Nature.) Digital photos and magnified SEM images of the hierarchical structure of the cactus (e)–(j), including trichomes, grooves, and barbs. Reproduced with permission.[36] (Copyright: 2012, Springer Nature.)

the Laplace pressure difference. This directional movement is similar to the cactus. The underlying principle is that the construction of different HS realizes a Laplace pressure difference and energy gradient to promote the directional movement of water droplets. The only difference is their HS. The HS are designed in real situations according to different demands.

3.2.3 A certain kind of fungi. Bionic materials have been developed for several decades. The aforementioned organisms are the most common bionic objects.[85,86] However, recently, some researchers have discovered that fungi have the ability to collect water from fog.[87] In 2022, Zhang *et al.* researched and proposed the structure of some fungi (*Rhizopus delmar*, *Mucor*

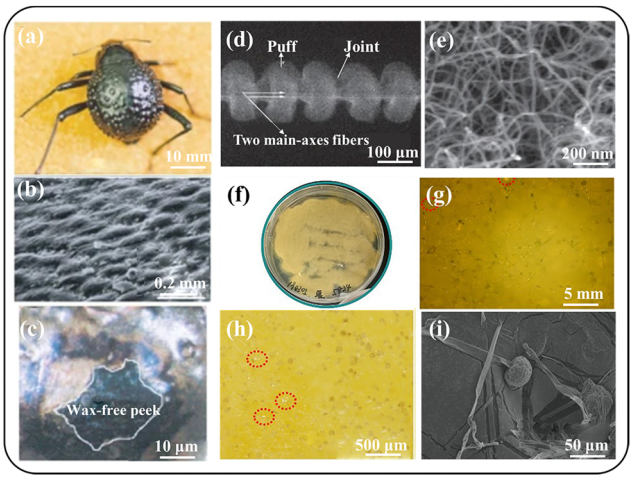

Fig. 4 Digital photos and SEM image of the SHL-SHB patterned surface of a Namib desert beetle. (a)–(c) Reproduced with permission.[58] (Copyright: 2001, Springer Nature.) SEM images of (d) and (e) spider silk. Reproduced with permission.[83] (Copyright: 2010, Nature.) Morphologies of fungi (f)–(i): optical image of fungi (f), stereomicroscopic image of fungi (g), light microscopic images of fungi (h), and SEM images of fungi (i).[88] (Copyright: 2022, the American Chemical Society.)

hiemalis f. hiemalis, and *Monascus purpureus*), and for the first time ingeniously fabricated a bioinspired HS material by mimicking fungi.[88,89] These fungi have the same common feature, *i.e.*, the existence of fibre-like mycelia on their surface. The interlaced mycelia are very similar to the spider web. The fungi have three layers, as follows: (1) the upmost layer consists of thin mycelia fibres and spores and (2) the middle and bottom layers are the thicker mycelia fibres, which require water for their growth, as shown in Fig. 4f–i.[88] The structure of the spores is similar to the spindle knots on the spider web, leading to a Laplace pressure difference. The spider web captures water through the hydrophilic nanofibers on the surface of spindle knots. Similarly, mycelia whether can alternate between hydrophilic and hydrophobic. Zhang's team further performed a fluorescence staining experiment and confirmed that the fungi (*Mucor hiemalis f. hiemalis*) are basically hydrophobic in total but possess obviously hydrophilic mycelia fibres to ensure that tiny droplets are collected, resulting in a wetting gradient to introduce small droplets converged into large droplets. Thus, mycelia such as the *Mucor hiemalis f. hiemalis* are amphiphilic.[90] Briefly, the ability of fungi to collect water is attributed to their web-like structure and HS, which are composed of an upper surface deposing fog and bottom surface draining water. Although mycelia are very similar to fibres, cultivated mycelia cannot be used as a raw material for manufacturing HS materials because of the difficulty in culturing them, low yield, *etc.* According to the above-mentioned analysis of the characteristics of the structure of fungi, it naturally comes to mind that designing HS materials inspired by fungi is a suitable alternative. There is also the possibility that HS materials can mimic fungi, while mimicking other organisms to acquire a better performance for collecting water.

Researchers rely on various technical methods to detect HS in organisms. Based on the relevant theoretical principles, the function of HS in organisms was discovered to form a foundation for FC applications.

4. The development of fog collection with hierarchically structured design

Biomimetic materials for FC do not necessarily contain HS. However, HS provides a basis for the development of FC.[91] Many biomimetic materials with HS have been successfully developed based on the function of HS for a specific process of FC in a typical organism, as described above.[92,93] Initially, after a deep understanding of the mechanism of FC in organisms that exhibit mist trapping, water coalescence, or water drainage, scientists have investigated biomimetic materials with HS. For example, using a simple wet chemical oxidation method, photolithography, and electron beam evaporation, Jiang[94] *et al.* prepared a patterned micro-bump (CuO) surface. This surface closely resembles the microstructure of the lotus leaf surface. Its specific HS is a CuO micro bump composed of CuO nano-whiskers. This bionic lotus leaf surface exhibited a good performance for the spontaneous removal of condensate droplets without overflow, demonstrating its potential application in fog collection. However, the efficiency of FC may be limited by this single bionic functional material with HS.[95] Recently, many research groups have developed ingenious strategies to combine some biomimetic materials with HS to achieve the synergy of the three processes of FC. Moreover, the combination of green energy sources (solar, wind, and turbidostatic) is also possible. In this section, from a bionic point of view, *i.e.*, from single bionic to multiple bionic approaches, an experimental case study is first analysed. From the perspective of spatial dimensions (one to three dimensions), the design of HS and their role are analysed based on bionics.

4.1 Single biomimetic design

4.1.1 One-dimensional design. One-dimensional (1D) design, which is linear and consists of innumerable points, always employs 1D materials. Thus, it is common for the majority of materials to imitate spider silk, which can efficiently harvest fog due to its HS, *i.e.*, spindle-knots and joints. Many groups have successfully fabricated silk-like materials through a series of methods, such as electrospinning,[96,97] fluid coating,[98] microfluidic spinning,[99] and dip coating,[100–102] and researched the factors impacting the their efficiency. Here, a single biomimetic can be based on specific organisms. However, many studies have also combined other organisms to enhance the efficiency of materials inspired by spider silk.

The materials inspired by spider silk are key to constructing a periodic roughness gradient (wettability gradient)[46,73] and curvature gradient (Laplace pressure difference).[39,103,104] In 2016, Zheng's group[105] considered this and conduct a study to find alternatives. They found that different solid/liquid contact areas can lead to as-modulated wet adhesion introduced by the orientations of spindle-knots on different strings obtained from experiments, where different sizes (length, pitch,

and height) of spindle-knots were fabricated to control the efficiency of FC. By adjusting the fluid velocity and the content of each component during the preparation of the fibres, the structure and morphology of the fibres can be effectively adjusted, and the spindle fibres with the best roughness and curvature radius can be obtained. When applied to mist collection, the surface of the spindle-knot microfiber captured tiny mist droplets, which then grew and coalesced with other mist droplets. Subsequently, the condensed droplets moved away from the centre of the junction such as a spindle knot. After the continuous directional movement of the coalesced droplets, the maximum volume of the droplets could overcome the adhesion force of the spindle knots and fall off from the spindle knots. In addition, the results also showed that the higher the spindle knot height, the larger the suspended volume at the moment of droplet shedding. In the case of the same length, a spindle knot with a larger width has a larger droplet suspension volume due to the longer contact line of the three-phase line.

Nevertheless, the size of the droplets is too tiny to timely move by the small Laplace pressure difference considering the size of the spindle-knots, resulting in the clogging of the surface capture sites.[106–108] In 2020, Zheng's group also ingeniously designed bioinspired nanofibril-humped fibres (BNFs) with HS, where the periodic spindle-knots were composed of interlaced random puff-like nanofibrils, and the joint consisted of aligned nanofibrils (parallel to the axis), by using the fluid coating method and electrospinning technique to resolve this problem (Fig. 5a).[109] The design of the HS mainly involved two dimensions. On the one hand, the interlace nanofibrils had two different states distributed inside the spindle-knots and joints, respectively (Fig. 5b). This design of fine HS not only realized a surface roughness gradient but also constructed channels inside the joints, transporting extremely tiny droplets introduced inside anisotropic capillary to resolve the above-mentioned problem, namely, inner transport. On the other hand, the outside of the fibres can complete FC similar to spider silk, namely, outer transport. The entire mechanism of the wetted fibres of FC is illustrated in Fig. 5c and d. When the dry artificial fibres were placed in a wetted environment, the hydrophilic fibres could capture tiny droplets because one of the components of the fibres is chitosan, whose structure has abundant hydroxyl, possessing hydrophilic properties. Next, the captured tiny droplets could be transported to the spindle-knots driven by capillary. The outside of the joints and spindle-knots could form droplets with different radii. The smaller droplet outside of the joints could be transported until coalescing with the bigger droplet outside of the spindle-knots driven by Laplace pressure difference. The two transporting modes, *i.e.*, outside and inside, are both closely related to HS. Thus, the cooperative effect of these two transporting modes resulted in the significantly improving efficiency of FC. Under conditions with the fog rate of 150 g s^{-1} m^{-2}, the FC efficiency of the spindle-knots was approximately 0.83 μL s^{-1} mm^{-2}. Similarly, the ability to hang water is vital to the performance of collecting water from fibers. However, this needs to be improved to enhance the efficiency of FC. This ability is affected by the capillary force, which is related to the length of the three-phase-line (TPL).[110,111] In 2022, Meng's group presented a novel design of HS, *i.e.*, spindle-knotted microfibers with continuous hollow channels, leading to larger capillary force compared with Zheng's design of microchannels, through a multiphase-laminar-flow microfluidic strategy, as shown in Fig. 5e, to construct the hollow structure, which is a novel way.[112] The aqueous two-phase system (ATPS) was introduced in the spinning process to form a stable laminar flow by injecting dextran with calcium (the inner phase) into polyethylene glycol (PEG) with sodium alginate (the middle phase). At the interface, Ca^{2+} was crosslinked with alginate to generate microfibers. Meanwhile, the HS, *i.e.*, hollow structure, was generated by preventing the alginate from spreading inward due to the high viscosity of ATPS. This was similar to the middle hollow structure, which had a strong shell to improve the stability of the microfibers. In addition, there was another HS, *i.e.*, the surface roughness of spindle-knots, the joints, and the connecting region between the spindle-knots and the joints, with small nanoparticles, wrinkles parallel to the axis, and smooth feature, respectively, as shown in Fig. 5f. Based on their experimental results, the ability to hang water and the efficiency of collecting fog both improved.

To date, most researchers only focused on the directional transportation of water on fibers.[113] However, in the five years, some groups focused on the reversibly directional movement of tiny droplets. Liu *et al.* designed a type of spindle-knot with HS *via* the double dip-coating technique in 2017.[114] They fabricated the fibres by combining polydimethylsiloxane (PDMS) and graphene with inherent HS because PDMS is a flexible material and the inherent chemical properties and structure of graphene have great potential to control the surface wettability. The mechanisms of this fog collection, which is related to the HS, are identical to the above-mentioned work. It is worth mentioning how complete reversible transport is realized. The major reason is that the HS can control the surface wettability. By laser etching, the surface of spindle-knots could be transformed into a hydrophobic surface. Simultaneously, the direction of gradient wettability changed, enabling the driving force of the wettability gradient to overcome the Laplace pressure difference to make the droplets move from the centre of the spindle-knots. This work is enlightening for the construction of smart materials whose surface performance can be transformed to face various realistic conditions under certain conditions.

In the flora and fauna, there are also organisms with a wire-like microstructure, helping to collect fog from the air. Besides spider silk, the wire-like microstructure of the plant pitaya was applied in FC.[115] This structure can significantly reduce the deviation of the mist flow, and the inherent hydrophilicity of the surface makes the mist gather in the form of water droplets. According to current research, there is no relevant design for HS that imitates the thorns of the plant pitaya. This may open new ideas for the preparation of 1D bionic HS.

4.1.2 Two-dimensional design. In two-dimensional (2D) designs, the main biomimetic objects are cactus, *Nepenthes alata*, lotus leaves, *etc.* The (HS) of these bionic 2D designs are based on the same principles as the (HS) of the 1D designs

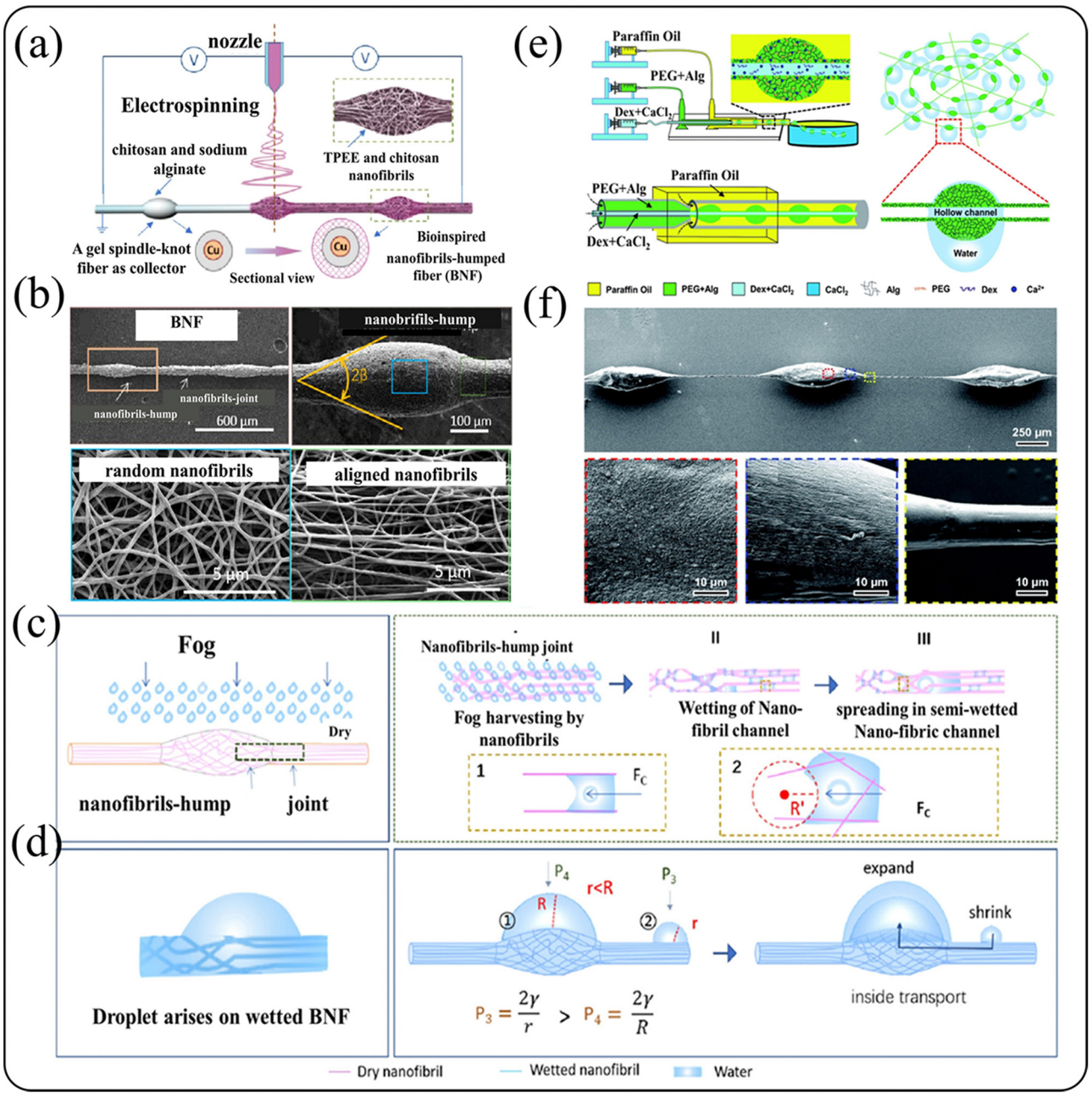

Fig. 5 One-dimensional design of a single bionic structure. (a) and (b) Schematic diagram of the fabrication of BNF *via* the electrostatic spinning of TPEE and CS nanofibrils and photos of the BNF and SEM images of a BNF with two nanofibril-humps, respectively. (c) and (d) Mechanism by which dry BNF with nanofibril-humps and joints under foggy conditions and redundant captured water arising as a droplet on the wetted BNF and tiny droplets are captured on the wetted nanofibrils and connect with the big droplet on the hump of the BNF by a water film (droplets ① and ②).[109] (Copyright: 2020, the American Chemical Society.) (e) Schematic of the microfluidic system for the preparation of HSFs and water collection. (f) SEM images showing the dehydrated microfiber.[112] (Copyright: 2022, The Royal Society of Chemistry.)

described above, which are constructing surface wetting gradients, Laplace pressure differences, and capillary forces. However, the 2D design requires a more imaginative approach to transform the three-dimensional structure of the bionic object into a 2D structure.[116,117] In addition, other functions can be achieved in the 2D design together with effective FC, such as surface antimicrobial and reduction of surface lubricant loss. Conical cactus spines can achieve efficient fog collection, but the fabrication of this type of 3D structure is complex and tedious. Cao[118] *et al.* designed a cactus kirigami, which simplified the cactus-inspired fog collection spines from a 3D cone to a 2D triangle, as shown in Fig. 6a. This design allowed the efficient capture of fog droplets and rapid reconfiguration of the collection interface by directed droplet self-propulsion. In this case, the HS was designed as follows: (1) a macroscopic 2D plane and (2) a 2D plane composed of many microscopic 2D

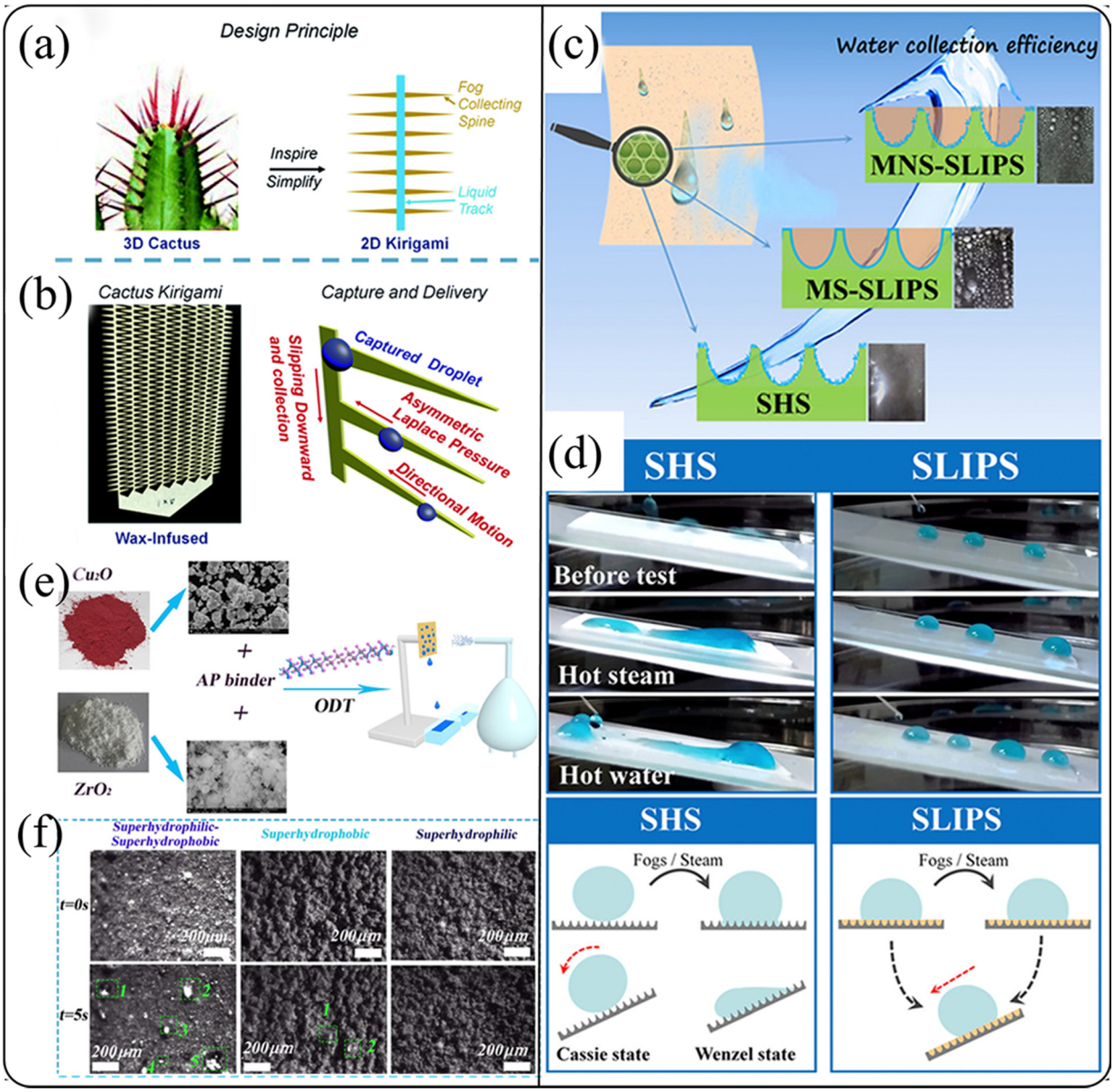

Fig. 6 Two-dimensional design of a single bionic. (a) and (b) The design of a cactus kirigami, and An optical image of a typical cactus kirigami with a dense arrangement of spines.[118] (Copyright: 2020 Royal Society of Chemistry.) (c) and (d) Schematic demonstrating slippery liquid-infused porous surfaces with HS, and hot-steam and hot-water resistance of SHS and SLIPS film.[119] (Copyright: 2020, American Chemical Society.) (e) and (f) Illustrating the preparation process of the biomimetic hybrid superhydrophilic–superhydrophobic surface, and comparison of fog capture capacity of the as-prepared hybrid superhydrophilic–superhydrophobic surface, superhydrophobic surface and superhydrophilic surface in 5 s (scale bar: 200 μm).[126] (Copyright: 2020, Elsevier.)

triangles (Fig. 6b). The 2D triangles were mainly designed to fulfil the function of cactus spines. Their hydrophobic spine, similar to the principle of Laplace pressure generated by the conical spine, could drive droplets from the tip to the root. The drops collected at the root then slid down a waxy track propelled by gravity into the collection container. For droplet self-propulsion at the millimetre scale, asymmetric structures such as triangles and cones, which can generate anisotropic Laplace pressure, are very useful. In addition, self-propulsion by Laplace pressure requires a sufficient droplet size, which requires the agglomeration of droplets. Also, this process often involves the release of the agglomeration energy, which allows the droplet to gain kinetic energy to overcome the droplet contact angle hysteresis at the spine surface. The macroscopic 2D plane is an amplification of the action of a 2D triangle to achieve efficient fog collection. The construction of this hierarchical structure eliminated the need for a cumbersome preparation process. It also greatly reduced the cost. When the fog flow velocity was about 220 cm s^{-1}, the FC efficiency was as high as 4000 mg cm^{-2} h^{-1}. However, although this 2D kirigami process is easy to operate and inexpensive, a more suitable method for the precise construction of HS still needs to be found.

In addition to the excellent water-harvesting function of cactus needles, the smooth liquid-injected porous surface (SLIPS) of *Nepenthes alata* can also harvest fog. However, the injected lubricant is usually unstable and easily depleted, which can lead to a decrease in the fog collecting efficiency and cause the collected water to be unsafe. Wang *et al.* developed a highly stable SLIPS with improved lubricant storage to collect fog inspired by *Nepenthes alata*, as shown in Fig. 6c.[119] Specifically, their designed HS was constructed as another nanoparticle structure in the constructed micro-pillow-shaped structure, which was also called micro-/nanostructures (MNS-SLIPS). The surface composed of HS had a better lubricant storage performance than the dimensionally textured surface.[120] According to their experimental results, it can be seen that the surfaces constructed by this method have extremely low water contact angles and water droplets can freely slide on them. In this work, the microporous structure was designed to retain the lubricant by capillary forces. Fig. 6d shows that after hot water treatment, the water droplet was better retained on SLIPS compared to the superhydrophobic surface (SS). Specifically, the presence of HS enabled the droplet to maintain the Cassie state on the constructed SLIPS. This could realize the process of continuous FC. In addition, this surface could be used for a long time and was highly resistant to hot steam and hot water, while enabling FC. Under the experimental conditions, the tested FC efficiency was 852 mg cm^{-2} h^{-1}, and preliminary experiments on the surface of this construction showed that it can work continuously for 20 h. In this work, the embodied HS did not directly affect the droplet motion in the fog collection. Instead, it maintained the stability of the surface material to maintain the continuity of the fog collection process. This is a method of indirectly maintaining the mist collection efficiency using HS. The designed HS can directly and indirectly improve the efficiency of FC simultaneously, which is a new approach that provides a different way of thinking for follow-up work.

The above-mentioned two methods for the construction of HS are similar in that the construction ideas are novel and the starting point for solving problems is different. In addition to plant biomimicry, related work on animal biomimicry has unique features. In animal biomimicry, the fog-collecting mechanism on the back of the beetle has received significant attention.[121,122] The alternately wettable surface on the back of the desert beetle has great potential for fog collection. Therefore, many researchers have been inspired by the desert beetle to prepare biomimetic materials for FC.[123–125] Guo's team successfully prepared a biomimetic surface with mixed wettability by using a simple spraying method and thiol-selective modification method, as shown in Fig. 6e.[126] Their HS design was a structure of hydrophobic microparticles/hydrophilic nanoparticles. The hydrophobic particles were Cu_2O particles modified with 1-octadecanethiol (ODT), and the hydrophilic nanoparticles were ZrO_2 nanoparticles, which were not modified with ODT. The test results of the FC ability of the prepared superhydrophilic/superhydrophobic surface, superhydrophobic surface, and superhydrophilic surface within 5 s (Fig. 6f) showed that this special HS can promote the fog collecting behaviour. The hydrophobic particles were large, the hydrophilic particles were small, and the hydrophilic points on the surface of the material were much smaller than the hydrophobic points. This was conducive to the adsorption of tiny water droplets on the surface. Simultaneously, it facilitated the transport of large amounts of water under the action of a surface wettability gradient. When the mass ratio of Cu_2O particles to ZrO_2 nanoparticles in the spray suspension was 8 : 1, the FC efficiency was up to about 1707.25 mg cm^{-2} h^{-1} (room temperature, relative humidity 90%).

In recent years, collectors related to biomimetic fog collection still cannot be manufactured on a large scale. Therefore, it is necessary to design a biomimetic fog-collecting material with HS that can be produced in a simple and low-cost way. Xie's research group proposed a method combining extrusion compression molding and surface modification for the large-scale fabrication of joint superhydrophobic-hydrophilic polypropylene/graphene nanosheet (UPP/GNS) films for FC, as shown in Fig. 7a.[127] The HS was based on the construction of desert beetle-inspired micropillars and nanoparticles (NPs) on the surface of UPP/GNS. The top of the micropillar was hydrophilic, and the bottom and sides were superhydrophobic. Fig. 7b illustrates the nucleation, coalescence, jumping, and aggregation processes of tiny droplets on the surface of the UPP/GNS-0.8 film. Initially, the droplets nucleated and formed tiny droplets on the hydrophilic tops of the micro-pillars and the superhydrophobic protrusions between the micro-pillars.[127] Also, the water droplets in the superhydrophobic region could jump after merging. The energy generated by jumping deformed them. The deformed droplet "a" came into contact with droplet "b" to form a liquid bridge, and then the bridge expanded rapidly, and the droplet began to shrink. As shown in Fig. 7c, the falling droplet "c" collided with droplet "d" and merged to form droplet "e". The energy generated by the collision was transferred to the bottom of the droplet, compressing the air between the nanostructures, and the droplet bounced back to the hydrophilic region under the reaction of the compressed air. In addition, droplet "e" was captured by droplet "f" in the hydrophilic region to form a large droplet "g". The droplets could be transported to the hydrophilic top due to the surface wettability gradient. Thus, the jumping water droplets were easily trapped on the hydrophilic top to facilitate water condensation and directional transport. In their experiments, the film was found to have excellent stability in harsh environments. This was mainly due to the mixed wettability of the UPP/GNS film surface and the construction of HS. Under their experimental environment, the efficiency of the obtained FC was 1251 mg cm^{-2} h^{-1}.

According to the preparation of materials with HS in the above-mentioned work, it can be seen that these related preparation methods often require complex processes. Also, some researchers focused on the inherent uniqueness of the HS in some organisms that plays the role of collecting water in the organisms. Crucially, these structures do not require complex processes, such as leaf veins and layered fibers in wood. Sharma *et al.* considered the pivotal role of leaf veins in water transport in plants, and inspired by leaf veins, proposed a leaf vein-like surface capable of the rapid nucleation, growth, and

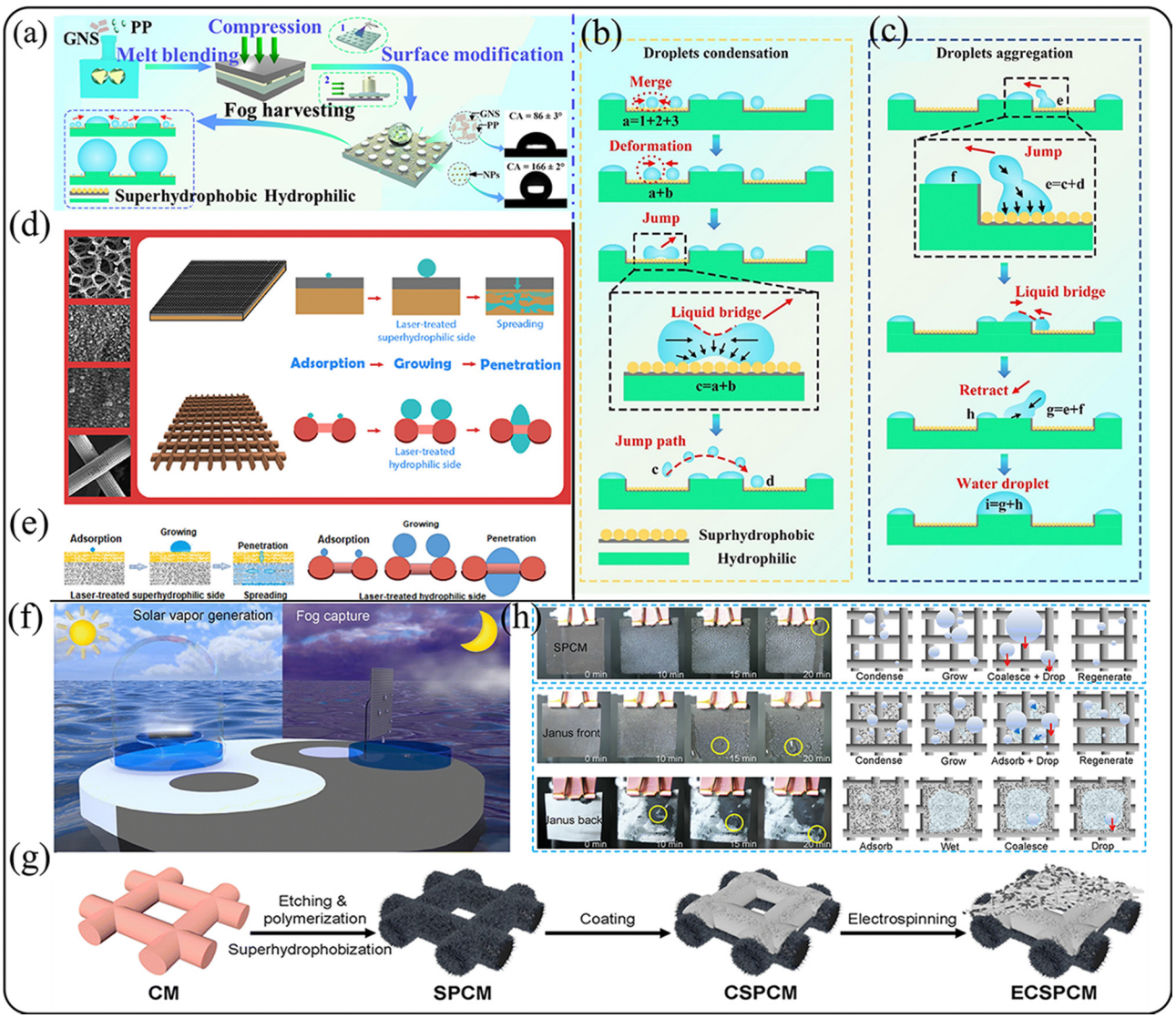

Fig. 7 Two-dimensional design of a single bionic. (a)–(c) Schematic illustration of the process for the preparation of UPP/GNS films; droplets condensation and, and aggregation on UPP/GNS-0.8 film surface.[127] (Copyright: 2023, Elsevier.) (d) and (e) Two types of materials used to fabricate membranes with asymmetric wettability behaviour: copper foam and copper mesh.[131] (Copyright: 2023, the American Chemical Society.) (f)–(h) Schematic demonstrating an asymmetrically superwettable Janus membrane for all-day freshwater harvesting.[134] (Copyright 2023, The Royal Society of Chemistry.)

directional transport of water droplets, which was combined on the skeleton of banyan leaf veins by electrodeposition and oxidation methods.[66] There were two main types of HS in this concept. Firstly, an HS imitating the vein structure of banyan leaves. Secondly, another hierarchical structure (CuO micro-clusters) constructed on each main vein. The ingenuity of this work was that the electrodeposition of copper on the irregular surface of the veins formed hills in the irregular spots, and after further oxidation, ''three-dimensional'' CuO micro-clusters were formed. This method can easily realize the construction of HS. This CuO micro-cluster structure facilitated the initial trapping and nucleation of droplets; the fractal structure on the main veins of the leaf facilitated the growth of the water droplets and the rapid movement of water; and the main vein structure of leaf facilitated the efficient transport and collection of water. The initial droplet nucleation sites provided by the CuO microstructure had high surface area microfibrils, which increased the probability of droplet-droplet coalescence. The fractal structure also ensured that the droplets coalesce or collide with each other to form larger droplets (pictured). This novel HS (controlled roughness microstructure combined with the unique fractal structure of the leaf skeleton) effectively synergized the fog collection process.

The 2D design often involves the construction of membrane-like materials. The name Janus membrane is derived from the ''two-faced god'' in ancient Roman mythology.[121,128,129] This design was inspired by the difference in wettability between the two sides of the lotus leaf. One of the most important properties of these membranes is their ability to manipulate and control fluid transport. In recent years, there has been a lot of

work on the use of Janus membranes to construct fog collecting materials. The reason for this is that Janus membranes can facilitate the transport of collected fog droplets without additional energy input. However, the commonly used membrane substrates require complex top-down fabrication processes or have poor mechanical properties, which limit their practical application. Ding *et al.* reported the fabrication of a wood-based Janus membrane.[130] Different from other works, the HS in this work and the surface wetting gradient (necessary for a Janus membrane) were inherent in the wood itself. This was because the wood had HS and was a bio-based, renewable, and mechanically robust material. The general procedure for making this film is to first vulcanize it with fluorosilane/TiO_2 nanoparticles, and then irradiate it with UV light on one side to create the required surface wettability gradient. Then, it is laser cut to obtain a thin wooden film and a surface with smooth HS on both sides. The experimental results showed that the water droplets adhered to the lower surface of the horizontally placed membrane. Although the hydrophobic surface was on the bottom, the water droplets were still transported to the hydrophilic surface on the top. This was driven by the Laplace pressure on the asymmetric wettable Janus membrane. The use of this natural internal HS offers great potential for future intelligent buildings in arid regions. The above-mentioned method for the construction of Janus membranes directly uses the advantage of the unique HS of wood. In addition, there are many other methods for the construction of Janus films using copper mesh. Alnaser *et al.* used two materials, *i.e.*, copper foam and copper mesh, and a femtosecond laser technique to construct two types of Janus films, as shown in Fig. 7d.[131] Femtosecond laser treatment[124] of one side of the membrane resulted in a superhydrophilic surface, while the untreated side remained hydrophobicity. Both membranes facilitated the easy transportation of the collected droplets from the hydrophobic side to the hydrophilic side and *vice versa*. It was clear that the HS was a result of the different wettability of the two sides and the micro-nanostructure of the surface constructed by the femtosecond laser. This superhydrophilicity of the surface is due to the increased surface roughness. In addition, it was also due to the large number of polar oxidation sites on the surface after femtosecond laser treatment, which had a strong affinity for hydroxylation. The structure of the Janus membrane constructed by the copper mesh was relatively simple, and a drop of water adsorbed on the hydrophobic surface passed directly through the lower side of the membrane. Also, in the foam, its internally intertwined structure made the water droplets diffuse to the internal hydrophilic part first, and then transport to the bottom (Fig. 7e). According to the experimental results, a reticular Janus membrane was obtained with higher fog collection efficiency than the copper foam-based Janus membrane. This femtosecond laser modification was not maintained for a long time and easily damaged, and thus it needed to be protected by certain hydrophilic coatings.

The high efficiency of the Janus membrane for harvesting fog is attributed to its hydrophobic upper surface, which reduces the flow resistance and promotes the collision of droplets and the aggregation of large droplets as well as their rapid transport to the hydrophilic regions.[132,133] Song *et al.* designed and fabricated a highly porous and asymmetric super-wettability Janus membrane that can be used for all-weather freshwater harvesting (Fig. 7f).[134] Its preparation is shown in Fig. 7g, where the copper mesh (CM) was chemically etched, and then modified as desired by coating to obtain a black copper mesh (SPCM) with a photothermal effect. Then, the chemical cross-linking reaction was carried out after coating to obtain compatibility between the asymmetric super-wettability layers (CSPCM). The final surface obtained by electrostatic spinning on the CSPCM surface was called ECSPCM, whose HS design was different wettability on both sides of the mesh and needle-like hydrophilic nanowires ($Cu(OH)_2$) on the copper mesh substrate. Fig. 7h compares the migration and collection of mist droplets on the surface of SPCM and the Janus membrane surface of ECSPCM. It can be seen from the results that the Janus membrane of the ECSPCM was able to capture smaller fog droplets. This was because the nanofibers with a superhydrophilic backside in the Janus membrane created a larger wetting gradient. In addition, the surface nucleation sites and specific surface area in contact with the fog increased by the hydrophilic nanowire structure present on the Janus membrane. The design of the HS structure in this work is popular, where it can capture fog at night, while allowing desalination during the day using a coating with a photothermal effect. This provides more ideas for the design of fog collectors, and the combination of certain chemical properties on top of the HS allows the efficiency of FC to increase to meet the daily water needs of humans.

4.1.3 Three-dimensional design. The HS previously designed by cactus-inspired researchers was three-dimensional (3D). The work on the design of this single-biomimetic 3D HS is an inspiration for today. It is also possible to use the ideas for the construction of HS in the present research. However, there are not many studies on this, and the design style may be rather homogeneous, given that most of the ideas are related to the imitation of the FC properties of the cactus.

Most of the work on cactus mimics focused only on the construction of wettability gradients on a conical surface, but not on the construction of graded grooved structures. Bai *et al.* produced artificial "cactus spines" with a grooved structure by electrostatic spinning and the sacrificial template method (Fig. 8a).[135] The main principle is the electrostatic spinning of a mixed solution of polystyrene (PS) and polyamide acid (PI). After imidisation, a large number of nanoparticles can be formed on the surface of PI due to the easy decomposition of PS. Therefore, PS is used as a template. The HS was a groove structure built on conical needles. This nano-groove structure could improve the droplet transport capacity. When the fog stream came in contact with the surface of the conical needle, the droplets were captured by the fibres inside the nano grooves and fused. The droplets prefer to be captured by the internal fibre bundles due to the presence of capillary forces. Simultaneously, the droplets on the spine surface could be driven by the Laplace pressure difference. In addition, the construction of HS on this conical needle changed the gas–liquid–solid TCL of the droplets on its surface, and a conical needle with HS divided the TCL into

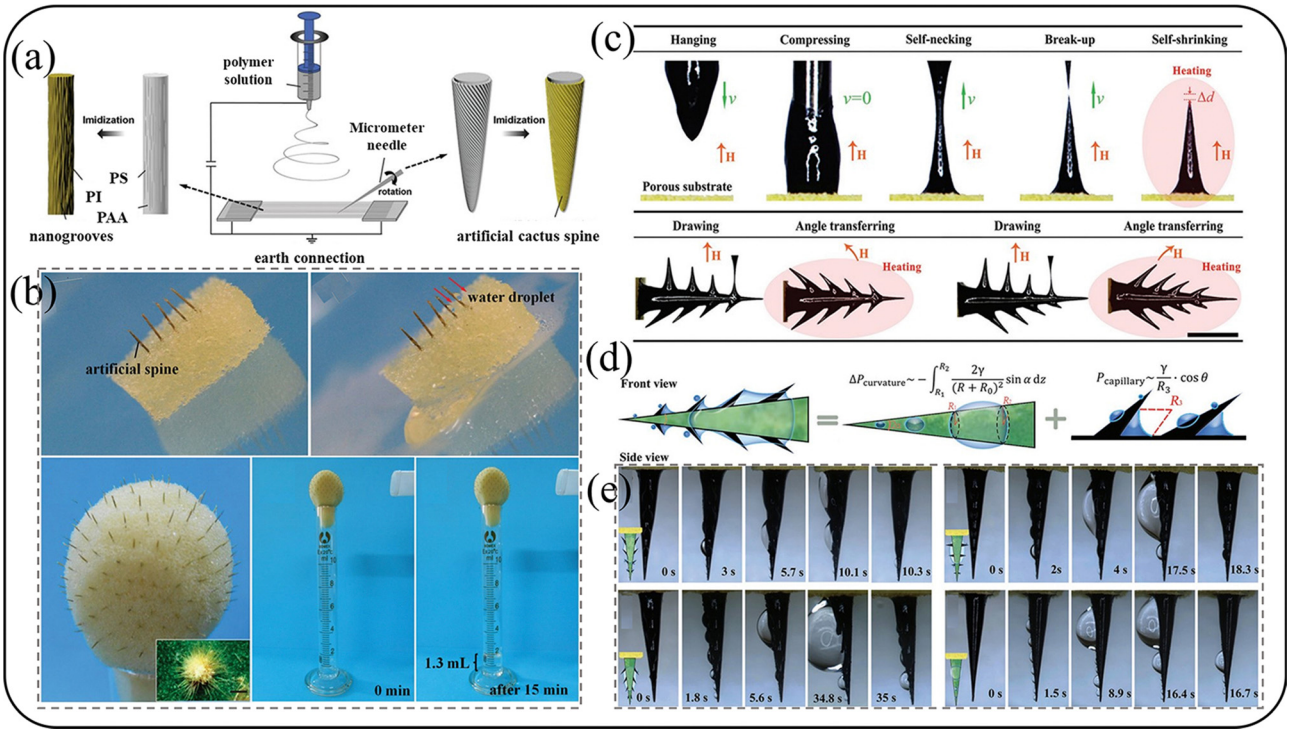

Fig. 8 Three-dimensional design of a single bionic. (a) Fabrication procedure of artificial cactus spine by combining ES with the sacrificial template method. (b) Fog collection test of an artificial spine array and the model of cactus equipped with 180 spines.[135] (Copyright: 2015, Wiley.) (c) Process for the fabrication of cactus-inspired spines with/without oriented microbarbs using the MRDL method. (d) Illustration of the mechanism of drop transport on the cactus. (e) Transport behaviour of droplets on a cactus-shaped cone with a backward reverse barb, vertical barb, front barb and no barb.[76] (Copyright: 2019, Wiley.)

several parts compared to a bare conical needle. This created a Laplace pressure difference on either side of the artificial spine. The presence of nano-notches could promote the formation of water droplets with a smaller radius. In this work, the Laplace pressure difference was effectively synergized with capillary action to improve the FC efficiency. Using a cactus model consisting of 180 artificial conical spines and spherical sponges, the model "cactus" could collect about 1.3 mL of fog in 15 min under a specific experimental environment (Fig. 8b). The conical needles of the cactus also had a directional micro-barb structure. This structure is also critical in the cactus fog harvesting system. Jiang's group observed the oriented barb structure of the cactus and came up with the idea of using magnetorheological mapping lithography (MRDL) to fabricate conical needles with an oriented barb structure (Fig. 8c). Employing this ingenious fabrication method, they successfully developed a conical needle with and without an oriented barb structure on a porous superhydrophilic substrate to achieve efficient fog collection.[76] It is clear that the HS involved in this work also has two dimensions. One is the conical needles. The Laplace pressure difference can be induced due to the different radii of the droplets collected on the conical needles. The other is the directional barb structure (Fig. 8d and e). The barb structure created a concave curved lunar surface between the barb and the spine, which induced capillary action. When the concave lunar surface came into contact with the fog stream, the tip of the conical spine captured small droplets and deposited the captured droplets. As the droplets coalesced, they gradually increased in size. Similar to other studies, droplet transport from the tip of the conical needle to the base of the conical spine was caused by the Laplace pressure difference, driven by the surface energy released by droplet binding. Once the droplet was transported to the bottom of the conical needle, the droplet was immediately absorbed by the hydrophilic porous substrate due to the differential wettability between the spine and the bottom substrate. Once this process was complete, the conical needle moved on to the next cycle of FC. In this work, a clever method of MRDL was used to construct the HS, and simultaneously, the HS enabled the synergy of several forces in the fog collection process to achieve efficient fog collection. Simultaneously, the risk of re-evaporation of the collected fog was reduced to some extent.

4.2 Dual biomimetic design

4.2.1 One-dimensional design. To overcome the limited application of a single bionic FC, researchers designed 1D finer HS inspired by spider silk together with other organisms by utilizing novel manufacturing methods.[136–138]

According to the above-mentioned analysis of single bionic-inspired spider silk, the design of the HS is always the different dispersion of inner fibres to complete the surface roughness gradient. In this case, the inner microstructure needs to be observed by more sophisticated instruments. If the larger surface roughness of the spindle-knots is constructed by surface fine HS, it can be easily observed and fabricated. Inspired by cactus spines

whose microstructure has the feature of gradient microgrooves and spider silk, Zhu *et al.* designed an improved HS, *i.e.*, spindle-knots and slender joints fibres with microgrooves, by implementing the flexible construction of multi-axial knotted microfibers through the parallel assembly of spinning nozzles, as shown in Fig. 9a.[139] This method for the construction of the HS involved a novel spinning technology, *i.e.*, dynamic interfacial spinning (DIS), whose principle is to utilize the controllable vibration of electrospinning at the air–liquid interface to produce microfibers with different morphologies.[140] The structure of microgrooves can offer a longer TPL and form capillary force, resulting in more efficient directional transport (Fig. 9b). Specifically, the tiny droplets can be ultrafast transported due to the effective synergy among the surface gradients, Laplace pressure differences, and capillary force. When the knot volume was 1.22 nL, the joint length was 268 μm, and when the fog flow rate was 0.53 mL min^{-1} cm^{-2}, the average fog harvesting capacity was 202.4 μL h^{-1} cm^{-1}. Compared with Zheng's design of channels between microfibers, this method can be more precise for the construction of microgrooves.

The process of fabricating artificial fibres is complex, but it is cheap. Although the structure of spider silk can readily cause directional transport, it is difficult to reproduce its spindle-knot structure *via* a straightforward method.[141]

Inspired by cactus spines, the conical structure is the same to realize directional transport. Seven years ago, Zheng's group designed a type of artificial conical copper wire with HS, which was fabricated by controlled electrochemical corrosion methods with periodic current gradients inspired by spider silk and cactus spines.[142] In this work, the HS mainly included the surface roughness difference in copper wires with gradients of the geometric curve. The surface roughness alternated between low roughness and high roughness, as shown in Fig. 9c. This HS design ingeniously combined the characteristics of spider silk (inducing surface-free energy gradient) and cactus spines (inducing Laplace pressure). Thus, the HS-inspired cactus spines and spider silk acted as a bridge to organically combine the wettability gradient, Laplace pressure, and droplet condensation energy. The schematic diagram in Fig. 9d clearly explains the harvesting-transport system. These conical copper wires were assembled in an FC collector, which exhibited the highest efficiency of around 0.36 mg s^{-1} under certain experimental conditions. This single bionic one-dimensional structure will eventually be assembled into a 2D collector to achieve efficient fog collection.

4.2.2 Two-dimensional design. To address the inherent limitations of efficient and large-scale water harvesting, Liu *et al.* were inspired by desert beetles and leaf vein wedges to fabricate a biomimetic fabric with a manipulable structure and

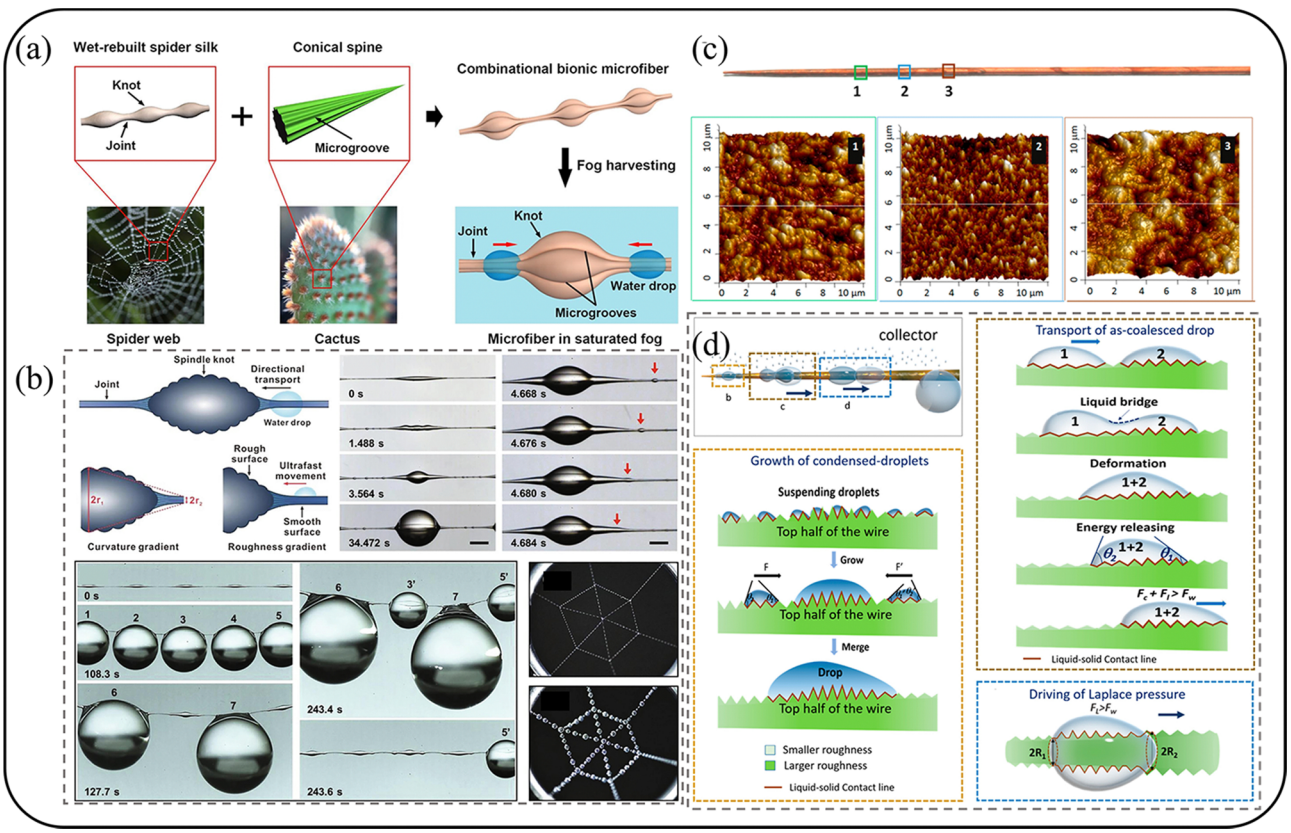

Fig. 9 One-dimensional design of dual bionic. (a) Combination of biomimetic microfiber (CBM) and knot-joint microstructure inspired by spider silk and surface microgrooves inspired by cactus spines for efficient fog harvesting. (b) Fog harvesting process of spider-silk-like microfiber.[139] (Copyright: 2022, Elsevier.) (c) Optical image of a representative periodic roughness-gradient conical copper wire (PCCW), and AFM images of different sites within one roughness period. (d) Illustration of fog collection on PCCW.[142] (Copyright: 2016, the American Chemical Society.)

wettability using a preparation technique, as shown in Fig. 10a.[143] In this case, the HS design was macroscopically a 2D leaf vein-like fabric. The leaf veins were divided into main veins and side veins. The main vein consisted of hydrophobic yarns and the side veins of hydrophilic yarns. The side veins were cross-linked with the main vein in the middle and formed a large number of wedge-shaped channels (Fig. 10b). The curvature gradient of this wedge-shaped channel created a Laplace pressure difference between the opposite sides of the captured droplets, which drove the captured droplets along the hydrophilic yarn to the hydrophobic yarn. These two HS designs combined droplet agglomeration, directional motion, and slip in a coordinated manner. The results of extensive parallel experiments showed that the efficiency of FC under this HS is 5424 mg h^{-1} cm^{-2}. Inspired by lotus leaves and beetles, Li's group developed a hydrophilic–hydrophobic/superhydrophilic unpaired lattice with a Janus structure for directional water transport.[144] Their test results showed that this HS (with alternating hydrophilic and hydrophobic surfaces and different wettability on both sides) can achieve a balance between fog capture and fog removal efficiency, and the maximum FC efficiency was measured to be 2478.73 mg m^{-2} h^{-1}.

Le *et al.* designed a novel HS-a spine with barbs and stratified channels (SBHC), as shown in Fig. 10c.[145] This HS could effectively combine the conical fog-trapping performance of micro-barbs in cacti with the rapid water transport performance of stratified microchannel ground trichomes in bottlebrush. This facilitated fog condensation or capture by focusing the vapor diffusion flow. In addition, the micro barbs on the spine increased the area for the fog deposition process and facilitated directional water transport. The hierarchical microchannels with high and low ridges automatically formed a thin film of liquid during fog collection for ultra-fast liquid transport. Two modes of droplet transport were performed in the SBHC compared with the spine with hierarchical channels (SHC), the spine with barbs and grooves (SBG), and the spine with bards (SB), as shown in Fig. 10d:[145] (1) water transport along dry layered microchannels and (2) water sloshing on a thin film of water. The driving force for ultrafast water transport in the primary channel in mode 1 was the capillary force and

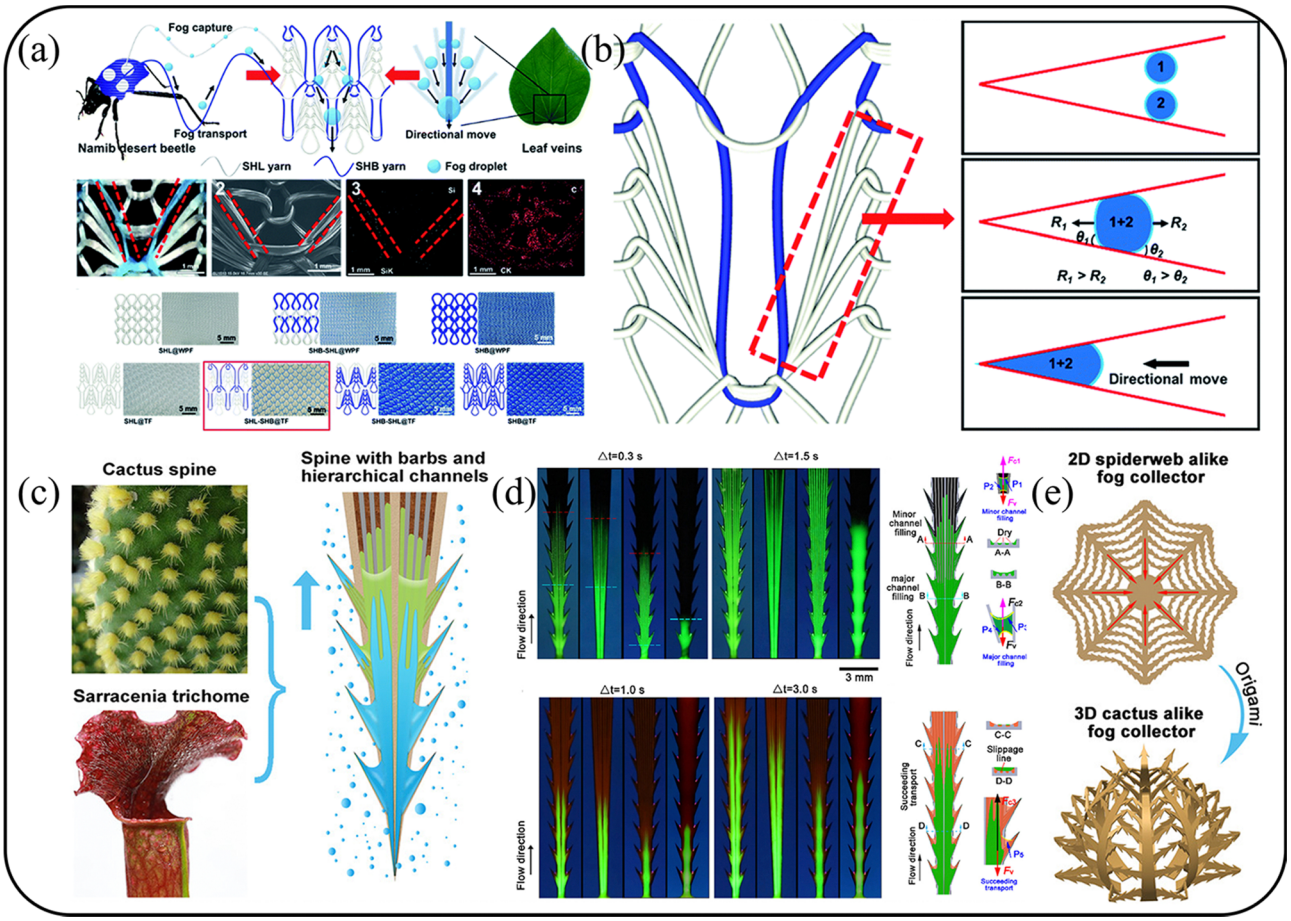

Fig. 10 Two-dimensional design of dual bionic. (a) Design and characterization of SHL–SHB@TF. (b) Schematic diagram of SHL–SHB@TF and force analysis of fog droplets on two adjacent fibers.[143] (Copyright: 2022, The Royal Society of Chemistry.) (c) Design of bioinspired spine with backward microbarbs and hierarchical microchannels for fog harvesting. (d) Water transport along dry different spines in mode 1 and corresponding to the schematic diagram of water transport along dry SBHC. Water slippage along wetted different spines in mode 2, corresponding to the schematic diagram of water transport along wetted SBHC. (e) 2D SBHC-based spider-web-like fog collector is turned into 3D SBHC-based cactus-like fog collector.[145] (Copyright: 2020, the American Chemical Society.)

the Laplace pressure difference induced by the collaborative spine shape of the layered microchannel. The capillary induced in the secondary channel was the main driver, while the micro-barb had little effect on water transport. In mode 2, the capillary forces generated by the concave curved lunar surface between the spine and the posteriorly oriented micro-barbs could drive water transport in mode 2. However, the 2D design does not allow for the collection of 360° fog in space. This work uses origami techniques to fold a two-dimensional spider web-like copper web into a three-dimensional cactus-like structure (Fig. 10e). The folded collector was tested in the experimental environment, where 2.8 mL of water was collected in 30 min. If ten of these devices were used in a day, they would provide the basic amount of water for an adult in a day. The trend today may be for 2D designs such as this to eventually be converted to 3D-collectors to increase the collection efficiency.

4.2.3 Three-dimensional design. Currently, most of the dual biomimetic HS designs being researched are 1D and 2D. However, in practice, 1D and 2D designs may limit the contact between the fog-collecting material and the fog.[146] Therefore, the direct design of 3D HS is important for practical applications.[147,148] However, in addition to being driven by Laplace pressure differences, wettability gradients, and capillary forces, the principle of designing 3D HS for fog collection is often driven by gravity.[149] Gravity-driven HS are often designed with an open surface, which increases the risk of the evaporation of the collected fog.[150,151] Cao's group proposed the design of a layered hydrophilic/hydrophobic (3H) surface with automatic surface extraction for fog collection, inspired by the multi-scale of cacti and the back of beetles.[152] There are 2D structures in the design of their HS. One is a conical needle with a hydrophilic/hydrophobic surface, while the other is a surface with a pattern. The conical needle with a hydrophilic/hydrophobic surface of the appropriate length enables anti-gravity transport, whereas a patterned surface is key to ensuring continuous FC. The combination of these two is essential for the continuous self-pumping of droplets.

To effectively increase the specific surface area of the droplets on the material surface, He *et al.* developed a 3D copper foam framework surface, which was synthesized with CuO nanoweb HS by combining the characteristics of cactus and pine needles.[153] Their HS was designed as a conical structure, a mesh structure, and a surface roughness structure. The conical structure could enable rapid droplet capture (driven by Laplace pressure and surface wettability gradient). The strong air confinement between the meshes facilitated rapid droplet shedding and provided multiple paths for droplet transport. In addition, the large specific surface area of the copper foam increased the contact area with the droplets. This HS design combined with copper foam resulted in a significant increase in FC. Under the experimental conditions, the highest collection rate of 4150 mg cm^{-2} was achieved in 120 s.

The special structure of the layered microchannels in the bottlebrush trichomes has an ultra-fast fog collection and transport pattern. This is due to its ability to induce the generation of capillary forces. However, the realizing the effect of multi-scale coupling of layered microchannels on efficient FC remains a major challenge. Chen *et al.* used a one-step thermoplastic stretching method to design bionic bottlebrush trichomes (BST) with on-demand layered microchannels on glass fiber bundles.[154] Their HS was designed with a primary channel confined by an internal gear pattern and a primary microchannel for the automatic assembly of glass fiber monofilaments. Simultaneously, it connected the BST vertically to a Janus membrane. Thus, the efficient fog collection in this work was due to the clever coupling of this novel HS to a Janus membrane, which enhanced the fog collection performance. As the BST surface dried, fog droplets condensed on its surface. These condensed droplets were collected and transported in spherical droplets along the trichomes. These droplets slid through and automatically formed a thin film of water on the layered microchannels. This created a liquid–liquid super-slip capillary force. Driven by the Laplace pressure difference and the capillary forces, high-efficiency FC was achieved. The collection based on the combination of BST and Janus membrane plates improved the fog collection performance by a factor of three compared to a single-scale structure.

The HS in the above-mentioned work are often designed to increase the specific surface area of materials, but few studies considered the electrostatic friction of the droplets as they come into contact with the material during the collection process. Zhang *et al.* were inspired by the remarkable features of cactus spines and Namibia desert beetle elytra wings to design an asymmetric amphiphilic surface for frictional, electrically enhanced fog harvesting and constructed a 3D collector.[155] The HS was a biomimetic cactus array and a coexisting hydrophilic and hydrophobic surface. The amphiphilic cellulose ester coating (ACEC) provided an effective nucleophilic site for droplets, where its hydrophobic component and asymmetric spines resulted in rapid droplet removal, while its hydrophobic channels with smooth interfaces avoided channel blockage. Innovatively, the collected droplets were used as a charge source to trigger a friction electric nanogenerator (D-TENG) for efficient fog collection (Fig. 11a and b). The detailed process of fog in this hierarchical structure is shown in Fig. 11c using microscopy, as follows: (1) the fog nucleates on an array of bionic cactus spines and (2) the nucleated droplets seek to move towards the root, fusing with neighbouring droplets. The good synergy of this process (Fig. 11d and e) is based on the graded structure of the hydrophilic surface combined with the cactus array.

4.3 Multiple biomimetic design

4.3.1 One-dimensional design. In 2021, Wang *et al.* introduced a novel HS inspired by the wettable pattern and gradient on the beetle and spider silk and multi-structure and hierarchical microchannels on the cactus and *Sarracenia* trichome *via* an innovative capillarity-induced selective oxidation method, as shown in Fig. 12a.[156] This work was an improvement based on the above-mentioned conical copper wires. They first dealt with the cone-tip of a row of copper wires to form a multi-structure, *i.e.*, "capturing area", by an electrochemical method inspired by cactus spines. Then, they inserted the other end into an electrolyte. The electrolyte could be transported in the microchannels

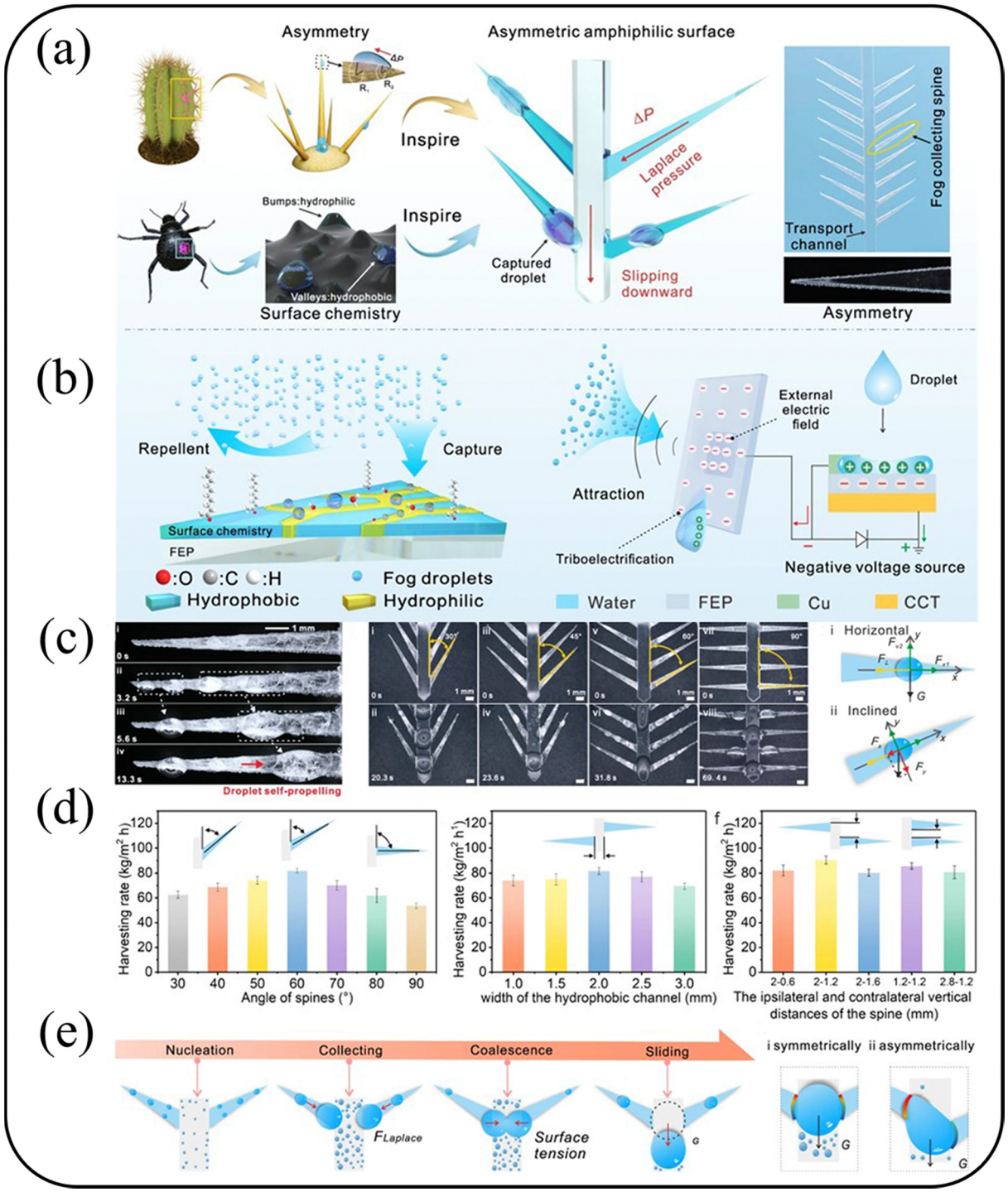

Fig. 11 Three-dimensional design of dual bionic. (a) and (b) Schematic illustration of asymmetrical smooth surface inspired by the asymmetry of cactus spines and the hydrophilic–hydrophobic surface of the beetle elytra. (c)–(e) Water-harvesting performance of dual structures and diagram of the water harvesting.[155] (Copyright: 2022, Nature.)

between copper (Cu) wires because Cu is hydrophobic. As the electrochemical process proceeded, the inner copper wires became more and more hydrophilic, which caused the liquid level of the electrolyte to continuously rise in the microchannels. The purpose of this process was that HS inside the microchannels could be formed to transport droplets, namely, the transport area, inspired by the wettable pattern of the beetle, wettable gradient of the spider, and microchannels in *Sarracenia*. The part of copper wires that were electrochemically corroded over 30 min could be oxidized to form copper hydroxide ($Cu(OH)_2$). $Cu(OH)_2$ has the characteristic of hydrophilicity. As shown in Fig. 12b, in the HS, the cone-tip was covered by hydrophilic nanowires, and

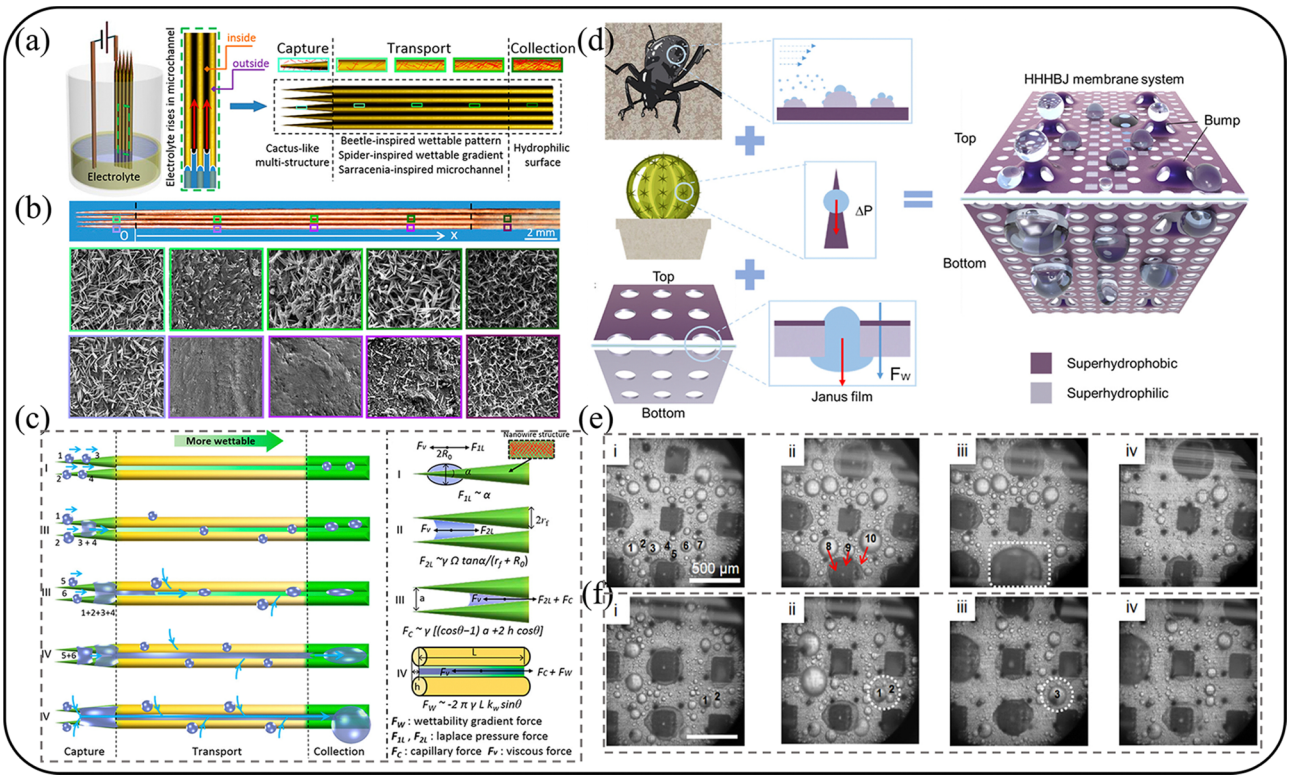

Fig. 12 One-dimensional design of multiple bionic: (a) process for the fabrication of an integrated bioinspired surface, where the surface can be divided into three areas, *i.e.*, capture, transport, and collection. (b) Optical image of the bioinspired integrated surface and SEM images on the different positions in the microchannel and outside the microchannel. The scale bar is 5 μm. (c) Illustration of fog harvesting process.[156] (Copyright: 2021, the American Chemical Society.) Two-dimensional design of multiple bionic. (d) Design strategy of the HHHBJ membrane system inspired by desert beetles, cactus spines, and Janus film. (e) and (f) Two types of dynamic droplet transferring modes of the TPJ film.[157] (Copyright: 2021, the American Chemical Society.)

the nanowires gradually became longer and denser. As shown in the schematic diagram in Fig. 12c, the fog droplets first were captured by hydrophilic nanowires on the surface of the cone tip. Enough big droplets could be driven by Laplace pressure until they were transported to the microchannels. The droplets in the microchannels could be transported by the wettability gradient and capillary force. The HS made by integrating the traits of multi-organisms could enhance the fog harvesting performance, which was 320% better than the ordinary samples (single bionic HS).[156]

4.3.2 Two-dimensional design. Inspired by the structural specificity of the backs of beetles, conical needles of cactus and the asymmetric wettability of lotus leaves, Su *et al.* fabricated a hierarchical hydrophilic/hydrophobic/bumpy Janus membrane (HHHBJ) *via* selective femtosecond laser ablation and chemical modification, as shown in Fig. 12d.[157] Unlike conventional Janus membranes, this work cleverly introduced hydrophilic and hydrophobic modes, while distributing the bumpy structure in a porous aluminium foil. Also, the present work achieved efficient FC mainly due to the constructed HS, which enabled a synergistic FC process. The uneven protrusions reduced the thickness of the boundary layer and allowed the fog stream to make effective contact with the surface of the structure. The hydrophilic zone allowed for faster droplet growth and the hydrophobic zone allowed for continuous fog water condensation. The hydrophilic square pattern on the film gradually increased the water film until it encountered the conical micropores by the combined forces of the chemical wettability gradient and Laplace pressure difference. The tapered micropores transported droplets in the hydrophilic region and spherical droplets in the hydrophobic region from the hydrophobic surface to the hydrophilic surface (shown as the white area in Fig. 12e and the white circle in Fig. 12f). Finally, the most interesting point of this work is the comparison of the fog collection performance of the different types of Janus films (Janus film, Janus film with hydrophobic patterns on the back, Janus film with hydrophilic patterns on the surface, Janus film with bumps and HHHBJ) characterized by the growth of soya bean shoots. It is clear from the graphs that HHHBJ has good mist water collection properties. Therefore, the effective design of HS is essential for the fog collecting performance.

The ever-improving HS only serve to increase the efficiency of fog collection.[158–160] Wang's group proposed a coupled HS borrowed from the alternately hydrophilic/hydrophobic patterned back of the desert beetle, honeycomb network structure of capillary channels and the unique microstructure of hogweed, *i.e.*, hydrophilic nanofiber protrusions, honeycomb network capillary channels and hydrophobic smooth matrix, based on which the HS was constructed using electrostatic spinning

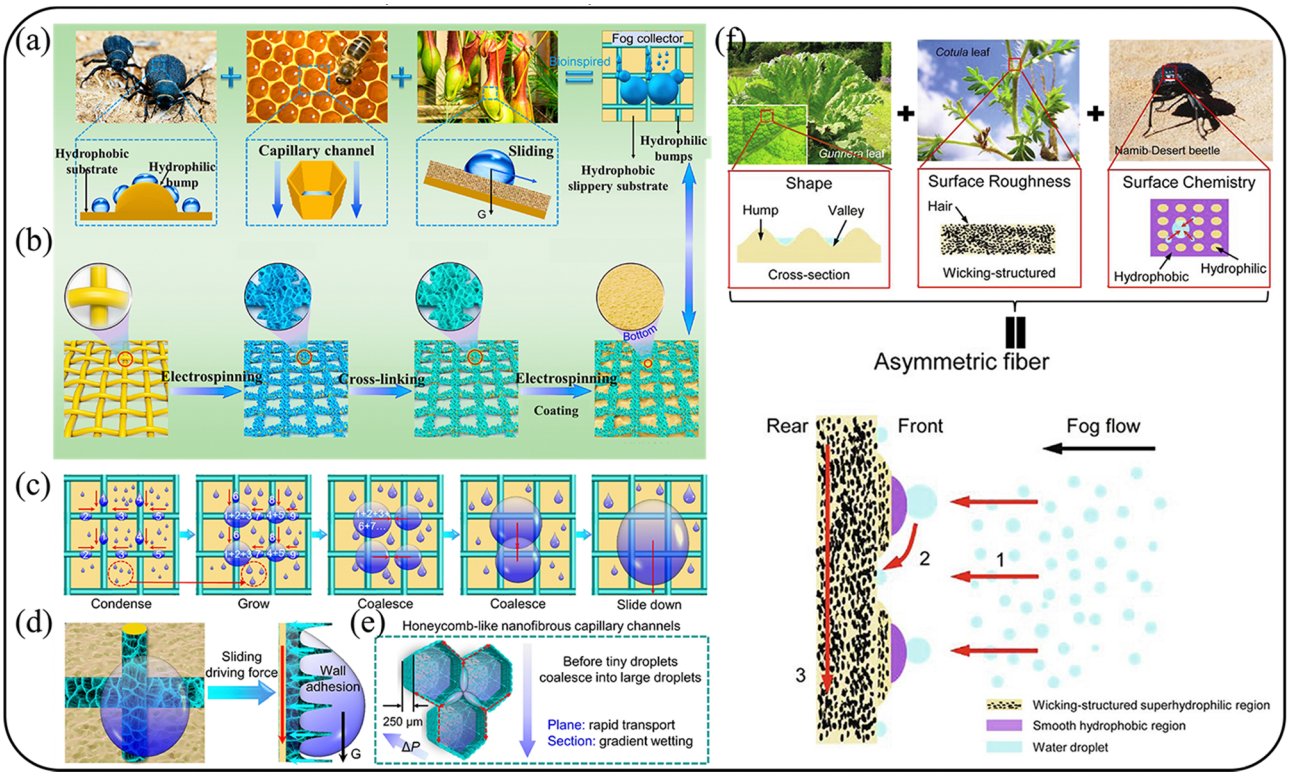

Fig. 13 Two-dimensional design of multiple bionic. (a) and (b) Scheme of the multi-bioinspired patterned fog collector by integrating the advantages of the hydrophilic–hydrophobic patterned back. (c)–(e) Illustration of fog condensation, water drop growth, coalescence, and directional sliding, and force analysis of the water drop during the sliding process.[161] (Copyright: 2021, the American Chemical Society.) (f) Design principle. Asymmetric fibers consist of periodic humps and valleys in the front inspired by *Gunnera* leaf, wicking fiber body inspired by hair of *Cotula* leaf, and alternating hydrophobic and superhydrophilic patterns inspired by Namib desert beetle, providing asymmetry in fiber shape, surface roughness, and surface chemistry for enhanced fog deposition (Process 1), fast water drainage (Process 3), and directional water transport from the front to rear (Process 2), respectively.[163] (Copyright: 2021, Elsevier.)

and electrostatic spinning coating methods to construct a lattice structure as shown in Fig. 13a and b.[161] The hydrophilic nanofiber protrusions promoted the trapping, growth, and agglomeration of droplets; the honeycomb capillary channels promoted rapid directional transport of agglomerated small droplets; and the smooth matrix was used to promote directional droplet sliding. Fig. 13c illustrates the droplet condensation, agglomeration and sliding in this work. To further illustrate the role of the honeycomb capillary channels, the forces generated by them were analysed in Fig. 13d. When the droplets met them, wall adhesion occurs due to the capillary effect, allowing the droplets to remain attached to the surface for a period. As the droplet agglomerated to a certain size, it met the smooth substrate, creating a sliding force. Fig. 13e also shows a small droplet orientation transport model for honeycomb nanofiber capillary channels to analyse the Laplace pressure difference between droplets on each honeycomb structure, driving droplet agglomeration. The above-mentioned analysis showed that the HS synergy achieved an integrated increase in FC efficiency. Under the experimental conditions, the FC efficiency was 1111 mg cm^{-2} h^{-1}. The Chen group developed a hybrid fog collector using 3D printing technology inspired by fog collecting systems of cactus, desert grass and *Nepenthes alata*.[162] The HS on this collector consisted of a cactus-inspired needle spike with longitudinal ridges and a curved, angled, curved crater decorating the bottom, inspired by desert grass and *Nepenthes alata*. The results of parallel design experiments showed that a fogging device with four conical needles with longitudinal ribs had the greatest effect on fog collection. Simultaneously, the design of the HS should be adapted to the actual situation.

Wang *et al.* observed that the rough structure of the *Gunnera* leaf enhanced fog deposition; the layered rough structure of the *Cotula* leaf allowed rapid drainage; and the desert beetle back promoted directional transport of fog droplets, constructing fibres with asymmetric shape, surface roughness and surface chemistry to enhance both fog deposition and drainage, as shown in Fig. 13f.[163] When the fog water contacted this material, its hydrophilic bumps trapped the droplets, as shown in Fig. 13f (1). A given volume of droplets deposited on the surface was transported from the concave side to the flat side, driven by a wettability gradient, as shown in Fig. 13f (2). The droplets transported to the flat side slid back down quickly, *i.e.*, drained in time, as shown in Fig. 13f (3). The coupling of the HS effectively synergized these three processes to achieve efficient mist collection and avoid evaporation of the collected water.

To reduce the risk of secondary evaporation of the captured droplets and increase the ability of materials to instantly capture fog, Lai's group designed a Janus composite with asymmetric

microtopography and anisotropy, inspired by the asymmetric microgeometry of cacti, the alternating hydrophobic/hydrophilic pattern on the back of desert beetles, the structure of spindle knots on spider silk, and the asymmetric wettability of lotus leaves.[164] Structural replication of the above-mentioned materials involved chemical etching and electrostatic spinning. The basic synthesis steps for this material are as follows: (1) ammonia-alkali etching of the copper mesh to produce a copper mesh with a homogeneous hydrophilic CuO micro-cluster structure and (2) electrostatic spinning (hydrophobic fibres with a spindle junction structure). The droplets were deposited on hydrophobic fibres (fibres with hydroxyl groups in their composition, which trap the droplets through hydrogen bonds between the hydroxyl groups and water molecules). Then, the droplets were directionally transported by the hydrophilic CuO micro-cluster structure or between them. It was important that droplets could only be transported from the hydrophobic side to the hydrophilic side. This HS reflects the cross-penetration properties that organically link the FC process. Simultaneously, the water retention rate was as high as 92.97% at 25 °C because the surface formed by the spun filaments could provide some protection against water evaporation.

Many water harvesting materials have been widely reported, but they are only suitable for certain application scenarios. Shi *et al.* constructed a novel layered multi-bionic membrane using a combination of carbon nanomaterials and polymer nanofibers, as shown in Fig. 14a,[165] mimicking the specific structures of termites, aquatic plants, fungi, spider webs and the back of desert beetles. The mechanism of fog droplet capture on this membrane fiber is shown in Fig. 14b. Tiny droplets in fog were captured by bumps of hydrophilic carbon nanospheres (HL-CNSs) on a single nanofiber, and when the droplets coalesced to a certain size, the droplets were stimulated by the high dynamic pressure generated by the bumps to slide down onto the hydrophobic nanofiber membrane (the mechanism of droplet capture on the back of a beetle is similar). The hydrophilic carbon nanotubes (HL-CNTs) created droplet adhesion properties (similar structure on termites) and the capillary forces between HL-CNS and HL-CNTs accelerated the condensation of the droplets. This is similar to the capillary forces that drive the spontaneous aggregation of floating particles, penetrating vegetation to the surface.[166–168] Fig. 14c shows that as the droplets continued to be captured, they spontaneously sank into the concave surface at a certain size, until they formed droplets large enough to overcome the adhesive forces on the surface and slid off. Fig. 14d shows that the droplets were successfully captured by the hydrophilic bumps regardless of whether they were moving at high or low speeds. To illustrate the role of the nanofiber mesh on the membrane in the FC process, Fig. 14e shows the movement of the droplet on the membrane surface. The mesh structure on the membrane surface could create an additional Laplace pressure difference between droplets on the membrane surface, which could drive droplet transport towards the hydrophobic region. Specifically, the HS could improve both the mist capture and transport efficiency by altering the wettability gradient and nucleation properties of the surface. The membrane had an FC efficiency of 1666.2 mg cm^{-2} h^{-1} and is reusable for long-lasting and efficient fog collection.

The fog harvesting materials developed at this stage are still weak in their ability to capture fog, transport fog droplets, and resist UV and mechanical damage.[169] Bo's group developed a Janus copper foam (CF) composite inspired by the surface structure of mussels and porcupine fish and the asymmetric wettability of lotus leaves.[121] The novel HS was an elastic needle-like skeleton similar to the porcupine fish structure and alternating hydrophobic/hydrophilic CF surfaces consisting of micron-sized tetrapod-like zinc oxide (T-ZnO) and PDMS. The large number of droplets trapped on the surface of the material continuously agglomerated, and driven by the Laplace pressure difference between the two sides of the material, the droplets could be spontaneously transported to the back side of the material. The general mechanism of fog collection is similar to that in previous work, but a more attractive aspect is that the HS design can maintain certain mechanical properties and achieve continuous FC with an FC efficiency of 1.7 g cm^{-2} h^{-1}.

4.3.3 Three-dimensional design. Inspired by the hierarchical microchannel water transport system of bottlebrush trichomes, the water harvesting system of cactus conical needles and the asymmetric wettability of lotus leaves, Chen *et al.* constructed a novel 3D-fog harvesting material, as shown in Fig. 14f.[170] The HS was designed with (1) hierarchical microchannels (HMC) with high and low rib structure on conical needles and (2) Janus membranes with bumps on the hydrophilic sides and conical pores. This team observed that the efficient water-harvesting capacity of the bottlebrush was mainly due to the presence of HMCs with high and low rib structures, combined with the efficient directional water transport capacity of the cactus conical needles, and thus designed conical needles with HMCs. To improve the ability to collect fog, the conical needle was coupled to a Janus membrane by means of a special projection on the Janus membrane. Simultaneously, conical holes were constructed to act as attachment points. Fig. 14g shows that the HS can be coupled to as many efficient collection mechanisms as possible. To demonstrate that the design of the HMC is critical, Fig. 14h shows that only structures with an HMC were able to agglomerate the airflow well enough to increase the contact between the microstructure and the airflow compared to the smooth (SS) and microchannel (MC) structures. Fig. 14i reflects the need for the timely transport of the agglomerated droplets in the HMC as the concave side of the wetted surface becomes convex without timely transport affecting the efficiency of fog collection. To demonstrate that rapid liquid transport can occur on the HMC, Fig. 14j divides the conical needle into a fog collection zone and a transport zone. As shown by the data plot in Fig. 14k, the HMC could maintain an efficient FC performance. The design of this HMC enables efficient synergy of capture-agglomeration-transport in FC applications. The new HMC needle conical pore Janus membrane coupled and integrated FC device is potential inspiration for FC applications.

Inspired by organisms with special wettability in nature, a series of fog collectors with HS have been developed (Table 1), providing new ideas for FC and beyond. The key to improving the efficiency fog collection is to optimise the synergistic

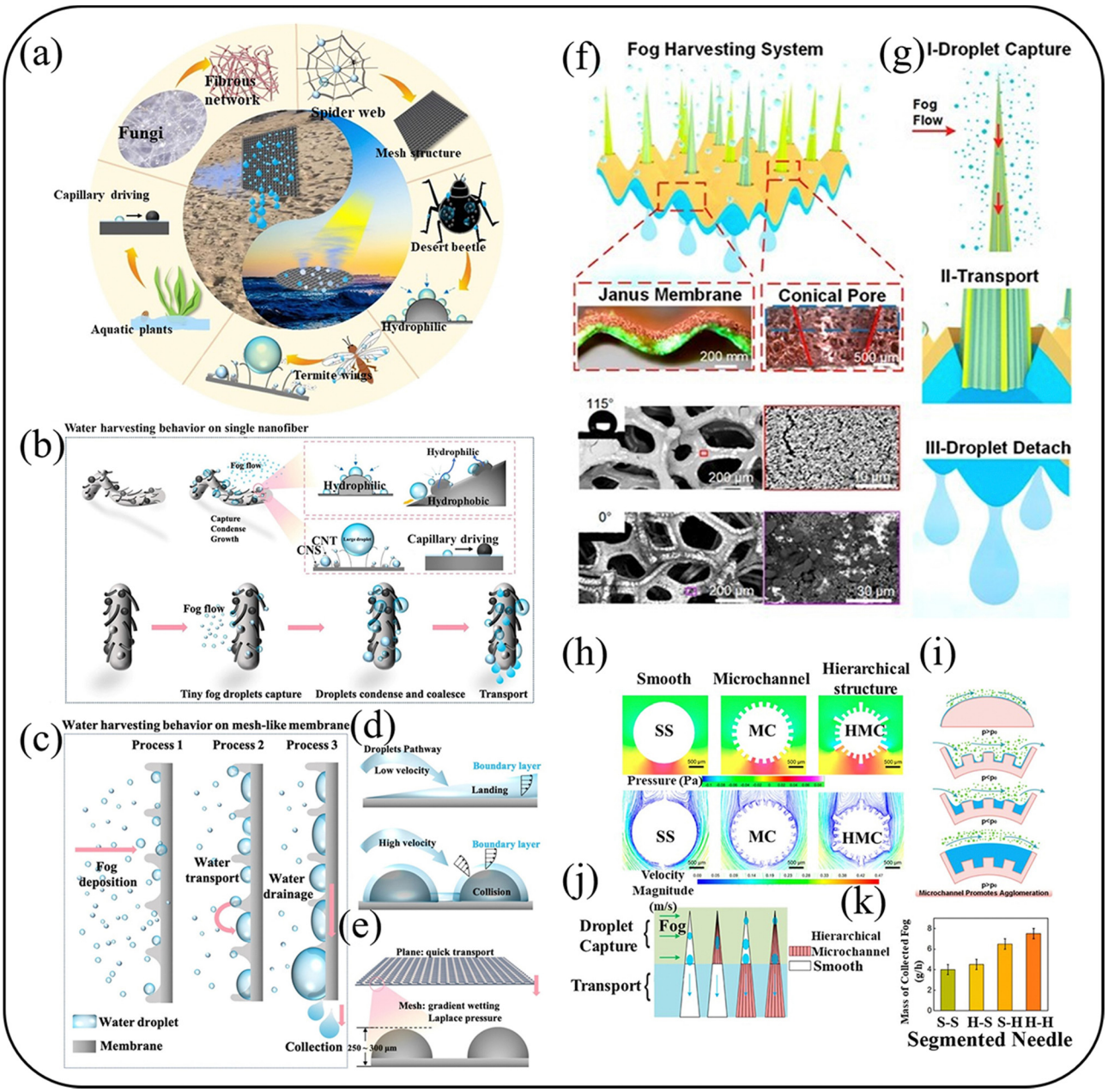

Fig. 14 Two-dimensional design of multiple bionic: (a) and (b) Scheme of the multi-bioinspired patterned fog collector by integrating the advantages of the hydrophilic–hydrophobic patterned back. (c)–(e) Illustration of fog condensation, water drop growth, coalescence, and directional sliding, and force analysis of the water drop during the sliding process.[165] (Copyright: 2022, Elsevier.) Three-dimensional design of multiple bionic: (f) Concept of the fog harvesting system and SEM images of the Janus membrane. (g) Progress of fog harvesting involving droplet capture (I), transport (II), and droplet detachment (III). (h) Simulation of pressure and flow velocity for needles with different profiles. (i) Microchannel promotes droplet agglomeration. (j) Exploring the role of microchannels in droplet capture and transport. (k) Mass of collected fog for the four segmented needles in (j).[170] (Copyright: 2022, the American Chemical Society.)

mechanisms of droplet capture, droplet aggregation and droplet transport. The HS can be designed to achieve efficiency improvements in one of the processes involved in FC. The most common HS design is used to modulate the wettability of the surface to achieve droplet transport through a wetting gradient.[171–173] In addition, a sophisticated HS is one that can synergise the three main processes of fog collection. Typically, the HS can enable multiple transport modes for the timely capture and rapid transport of small droplets. For instance, liquid bridges can be constructed through HS to enable droplet capture, droplet aggregation, and droplet transport to occur almost simultaneously.[127] Thus, a rational HS structure acts as a bridge between the three processes of FC. In recent years, the development of materials for fog collection tended towards multiple bionics due to the limitations of single bionic and dual bionic HS designs for fog collection. Simultaneously, much work has been inspired by

Table 1 The research progress of representative HS designs for FC

	Biomimetic objects	Dim	The design of HS	Force of FC	Fog flow	FC rate	Ref.
Single bionic	Wetted spider silk	1D	Periodic humps composed of interlaced random nanofibrils and a joint composed of aligned nanofibrils	Capillary force, Laplace pressure difference	150 g s^{-1} m^{-2}	Related to the number of BNF and temperature	109
	Spider silk	1D	Spindleknotted microfibers with continuous hollow channels, and surface roughness	Gravity and capillary force	1 mL min^{-1}	35.65 μL min^{-1}	112
	Cactus spines	2D	Triangular spines and liquid track	Asymmetric Laplace pressure and gravity	220 cm s^{-1}	4000 mg cm^{-2} s^{-1}	118
	Desert beetle	2D	Surface with micro/nano structure (micropillar with hydrophilic top and superhydrophobic bottom and sidewall)	Wetting driving force	—	1251 mg cm^{-2} h^{-1}	127
	Lotus leaves	2D	Highly porous and asymmetric super-wettability Janus	Wetting gradient, gravity	—	11.31 kg m^{-2} h^{-1} (nighttime)	134
	Cactus	3D	Conical needles with hierarchical groove structure	Internal capillary force, Laplace pressure difference	—	0.3 μL min^{-1} (single spine)	135
	Cactus	3D	Conical spines with an oriented barb	Laplace pressure gradient, capillary force, and wettability of the superhydrophilic porous	—	237 mg h^{-1} (spines with backward barbs)	76
Dual bionic	Cactus, spider silk	1D	Spindle-knots with microgrooves, and slender joints	Capillary force	0.53 mL min^{-1} cm^{-2}	202.4 μL h^{-1} cm^{-1}	139
	Spider silk, cactus	1D	Surface roughness difference, gradient of the geometric curve	Surface-free energy gradient, Laplace pressure	1.8 m s^{-1}	0.36 mg s^{-1}	142
	Desert beetle, leaf vein wedges	2D	Leaf vein like fabric with main vein of hydrophobic yarns and side vein of hydrophobic yarns	Laplace pressure difference, wettability gradient	—	5424 mg h^{-1} cm^{-2}	143
	Cactus spine, *Sarracenia* trichome	2D	Spines with barbs and hierarchical microchannels	Laplace pressure gradient, capillary force	—	5 mL h^{-1}	145
	Cactus, desert beetle	3D	Asymmetric amphiphilic surface	Laplace pressure difference, gravity	300 mL h^{-1}	93.18 kg m^{-2} h^{-1}	155
Multiple bionic	Desert beetle, spider silk, cactus, *Sarracenia* trichome	1D	Conical copper wires with wettable pattern and gradient, and hierarchical microchannels	Laplace pressure, wettability gradient, capillary force	0.8 m s^{-1}	2.48 g h^{-1}	156
	Desert beetle, cactus spines, lotus leaf	2D	Hierarchical hydrophilic/hydrophobic/bumpy Janus membrane	Wettability gradient, Laplace pressure difference	~40 cm s^{-1}	0.19 g min^{-1}	157
	Desert beetle, honeycomb, pitcher plant (*Nepenthes alata*)	2D	Hydrophilic nanofibrous bumps with honeycomb-like cellular grid structure, hydrophobic slippery substrate	Laplace pressure difference, wettability gradient, gravity, sliding driving force	—	1111 mg cm^{-2} h^{-1}	161
	Gunnera leaf, *Cotula* leaf, desert beetle	2D	Fabric with superhydrophilic wicking-structured region and smooth hydrophobic region	Wettability gradient, gravity	—	1.07 L m^{-2} day^{-1}	163
	Desert beetle, spider web, Fungi, aquatic plants, Termite wings	2D	Janus membrane with mycelia-like structure, mesh-like structure, irregular hydrophilic bumps, hair-like structure	Laplace pressure difference, wettability gradient	40–50 cm s^{-1}	1666.2 mg cm^{-2} h^{-1}	165
	Bottlebrush trichomes, cactus spine, lotus leaf	3D	(1) Hierarchical microchannels with high and low rib on conical spines, (2) Janus membranes with bumps on the hydrophilic sides and conical pores	Laplace pressure difference, wettability gradient	0.35 m s^{-1}	3.8 ± 0.2 g (in 20 min)	170

bionic work, developing a range of functions without an explicit bionic goal, which is referred to as indirect bionics.[174–177] Many of the HS designed by this indirect bionic work also involve the simulation of HS in multiple organisms.[178,179] The construction of a multibiometric HS requires the coupling of several different structures using appropriate methods.[180–182] It is clear from this work on the construction of multi-mimetic HS that the performance in terms of fog collection and avoidance of water evaporation is relatively good. However, there are still some disadvantages of multi-biomimetics.[183] Firstly, the design associated with multi-bionic HS is more difficult. Secondly, multi-mimetic HS are often complex and need to be constructed using sophisticated methods. This makes the cost of constructing these materials uneconomical. Thirdly, there is the problem that multi-bionic-related HS cannot be produced in large quantities. When analysed again in the spatial dimension, it is clear that 3D design-related work can easily meet the needs of practical applications. Furthermore, a current trend is to convert 1D HS designs into 2D or 3D collectors, or 2D HS designs into 3D collectors. This conversion idea satisfies both the simple design of HS and practical applications. 3D designs are good, but 3D designs require a very clever design. This makes them more difficult to build. In addition, 3D design often needs to consider mechanical properties. Given that the external environment is variable, especially today when extreme weather conditions are common, collectors need to be extremely adaptable to the environment. However, the 3D collectors developed at this stage are not yet able to meet this mechanical performance requirement. Nonetheless, the current phase of bionic HS-related design is in some ways an inspiration and blueprint for later work.

5. Conclusion and future prospects

Water, according to Leonardo da Vinic, is where life begins. However, water scarcity is one of the greatest threats facing humanity today. This is compounded by global warming, which has made already water-scarce regions even more vulnerable. Ice in the Arctic and Antarctic regions is melting hundreds of times faster than before, making the development of fog harvesting even more important. Consequently, there is an urgent need to develop low-cost, high-performance, mechanically efficient and easy to use fog harvesting materials. Herein, we initially discussed the basic principles of fog harvesting. Secondly, the role of HS in fog water harvesting was analysed in the microstructure of typical examples of plants and animals. Simultaneously, the fog-harvesting function of HS in a relatively new organism, fungal filaments, was also presented. Finally, the HS design in each representative work was analysed from a biomimetic perspective (single to multiple biomimetic). Then, the role of HS in fog harvesting and the fog harvesting performance of each work were analysed in order of spatial dimension from a bionic perspective. Although FC has been developed over many years and many unique HS have emerged, there is still the problem that they are not commercially viable. In addition, fog harvesting related materials also present the following challenges:

(I) The design of HS related to fog harvesting also needs to be more applicable to practical situations, *i.e.*, flexible and versatile. For example, the designed 1D HS material can be transformed into a 3D collector.

(II) The constructed HS is susceptible to damage. For example, chemically etched micro-nano clusters are easily depleted in practical applications.

(III) The FC using the constructed HS requires a simpler method of operation. At this stage, if the construction method is simple, the experimental equipment involved is relatively expensive.

(IV) There are no clear criteria for quantifying the performance of materials related to fog collection, such as the fog collection environment (temperature and humidity) and the fixed area of the fog collection material.

(V) The mechanism of action of certain HS designs in the fog collection process is not robust.

(VI) The relevant parameters in the HS of fog collecting designs are not yet clear.

Regarding the aforementioned challenges, it is evident that the commercial availability of fog collectors with bionic hydrophobic surfaces is hindered by their cost, design complexity, and mechanical properties. To construct precise HS, advanced instruments are vital, and consequently, the fog collector can be integrated with other applications to broaden its practical usability. This will enhance its practical worth. Nowadays, FC and desalination, FC and hygroscopic power generation, and FC and droplet friction generators are common joint applications. These areas have seen a surge of research interest in recent years. Additionally, HS are critical components of fine structures. To determine their optimal mechanical strength, relevant parameters must be set, and the HS need to be designed accordingly for experimental testing. Therefore, it is essential to reasonably design the HS.

Fog harvesting is a reliable and effective means for solving the water scarcity problems. The construction of novel and effective HS will open up new approaches for the future widespread commercial application of fog harvesting. In the future, it is expected that efficient FC can be achieved, while simultaneously absorbing excess carbon dioxide from the Earth to achieve 'carbon neutrality'.

Conflicts of interest

The authors declare no conflict of interest.

Acknowledgements

This work was financially supported by the National Nature Science Foundation of China (no. 51735013).

Notes and references

1 T. Bernauer and T. Böhmelt, *Nat. Sustainability*, 2020, **3**, 350–356.
2 B. Wang, X. Zhou, Z. Guo and W. Liu, *Nano Today*, 2021, **40**, 101283.

3 B. Bhushan, *Philos. Trans. R. Soc., A*, 2020, **378**, 20190440.
4 A. Feng, N. Akther, X. Duan, S. Peng, C. Onggowarsito, S. Mao, Q. Fu and S. D. Kolev, *ACS Mater. Au*, 2022, **2**, 576–595.
5 Y. Tu, R. Wang, Y. Zhang and J. Wang, *Joule*, 2018, **2**, 1452–1475.
6 S. Korkmaz and İ. A. Kariper, *Environ. Chem. Lett.*, 2019, **18**, 361–375.
7 Y. Guo, H. Lu, F. Zhao, X. Zhou, W. Shi and G. Yu, *Adv. Mater.*, 2020, **32**, e1907061.
8 F. Zhao, Y. Guo, X. Zhou, W. Shi and G. Yu, *Nat. Rev. Mater.*, 2020, **5**, 388–401.
9 Q. Yan, Y. Bi, Y. Deng, Z. He, L. Wu, J. D. Van Nostrand, Z. Shi, J. Li, X. Wang, Z. Hu, Y. Yu and J. Zhou, *Sci. Rep.*, 2015, **5**, 8605.
10 M. Zhu, Y. Li, G. Chen, F. Jiang, Z. Yang, X. Luo, Y. Wang, S. D. Lacey, J. Dai, C. Wang, C. Jia, J. Wan, Y. Yao, A. Gong, B. Yang, Z. Yu, S. Das and L. Hu, *Adv. Mater.*, 2017, **29**, 1704107.
11 A. Kumar, K. R. Phillips, G. P. Thiel, U. Schröder and J. H. Lienhard, *Nat. Catal.*, 2019, **2**, 106–113.
12 H. Frumkin, M. B. Das, M. Negev, B. C. Rogers, R. Bertollini, C. Dora and S. Desai, *BMJ*, 2020, **371**, m2936.
13 S. W. Cooley, J. C. Ryan and L. C. Smith, *Nature*, 2021, **591**, 78–81.
14 J. Yang, S. Kang, D. Chen, L. Zhao, Z. Ji, K. Duan, H. Deng, L. Tripathee, W. Du, M. Rai, F. Yan, Y. Li and R. R. Gillies, *Nat. Commun.*, 2022, **13**, 7360.
15 E. Mulcahy, *BMJ*, 2022, **377**, o1481.
16 Z. Yu, T. Zhu, J. Zhang, M. Ge, S. Fu and Y. Lai, *Adv. Funct. Mater.*, 2022, **32**, 2200359.
17 X. Liu, D. Beysens and T. Bourouina, *ACS Mater. Lett.*, 2022, **4**, 1003–1024.
18 F. T. Malik, R. M. Clement, D. T. Gethin, W. Krawszik and A. R. Parker, *Bioinspiration Biomimetics*, 2014, **9**, 031002.
19 R. T. Bruintjes, *Bull. Am. Meteorol. Soc.*, 1999, **80**, 805–820.
20 X. Dai, N. Sun, S. O. Nielsen, B. B. Stogin, J. Wang, S. Yang and T.-S. Wong, *Sci. Adv.*, 2018, **4**, eaaq0919.
21 M. Fessehaye, S. A. Abdul-Wahab, M. J. Savage, T. Kohler, T. Gherezghiher and H. Hurni, *Renewable Sustainable Energy Rev.*, 2014, **29**, 52–62.
22 Z. Wang, M. Elimelech and S. Lin, *Environ. Sci. Technol.*, 2016, **50**, 2132–2150.
23 R. T. Bruintjes, *Bull. Am. Meteorol. Soc.*, 1999, **80**, 805–820.
24 T. P. DeFelice and D. Axisa, *Atmos. Res.*, 2017, **193**, 173–183.
25 M. A. Muñoz-García, G. P. Moreda, M. P. Raga-Arroyo and O. Marín-González, *Comput. Electron. Agric.*, 2013, **93**, 60–67.
26 G. Sharan, A. K. Roy, L. Royon, A. Mongruel and D. Beysens, *J. Cleaner Prod.*, 2017, **155**, 83–92.
27 A. F. Batisha, *Sustainable Water Qual. Ecol.*, 2015, **6**, 1–10.
28 G. Raveesh, R. Goyal and S. K. Tyagi, *Energy Convers. Manage.*, 2021, 239.
29 J. Knapczyk-Korczak and U. Stachewicz, *Nanoscale*, 2021, **13**, 16034–16051.
30 S. Montecinos, D. Carvajal, P. Cereceda and M. Concha, *Atmos. Res.*, 2018, **209**, 163–169.
31 Z. Chen, L. Dong, D. Yang and H. Lu, *Adv. Mater.*, 2013, **25**, 5352–5359.
32 M. J. Kalmutzki, C. S. Diercks and O. M. Yaghi, *Adv. Mater.*, 2018, **30**, 1704304.
33 Y. Song, N. Xu, G. Liu, H. Qi, W. Zhao, B. Zhu, L. Zhou and J. Zhu, *Nat. Nanotechnol.*, 2022, **17**, 857–863.
34 Y. Zhang, T. Wang, M. Wu and W. Wei, *Surf. Coat. Technol.*, 2021, **419**, 127279.
35 H. G. Andrews, E. A. Eccles, W. C. Schofield and J. P. Badyal, *Langmuir*, 2011, **27**, 3798–3802.
36 J. Ju, H. Bai, Y. Zheng, T. Zhao, R. Fang and L. Jiang, *Nat. Commun.*, 2012, **3**, 1247.
37 Y. Shi, O. Ilic, H. A. Atwater and J. R. Greer, *Nat. Commun.*, 2021, **12**, 2797.
38 T. Young, *Philos. Trans. R. Soc. London*, 1805, 65–87.
39 N. W. Robert, *Ind. Eng. Chem.*, 1936, **28**, 988–994.
40 G. Whyman, E. Bormashenko and T. Stein, *Chem. Phys. Lett.*, 2008, **450**, 355–359.
41 A. Cassie and S. Baxter, *Trans. Faraday Soc.*, 1944, **40**, 546–551.
42 N. A. Patankar, *Langmuir*, 2004, **20**, 8209–8213.
43 X. Liu and P. Cheng, *Int. J. Heat Mass Transfer*, 2015, **83**, 842–849.
44 P. Ge, S. Wang, J. Zhang and B. Yang, *Mater. Horiz.*, 2020, **7**, 2566–2595.
45 C. Furmidge, *J. Colloid Sci.*, 1962, **17**, 309–324.
46 S. Daniel, M. K. Chaudhury and J. C. Chen, *Science*, 2001, **291**, 633–636.
47 L. Lorenceau and D. Qur, *J. Fluid Mech.*, 2004, **510**, 29–45.
48 D. Gurera and B. Bhushan, *J. Colloid Interface Sci.*, 2019, **551**, 26–38.
49 H. C. Yang, J. Hou, V. Chen and Z. K. Xu, *Angew. Chem., Int. Ed.*, 2016, **55**, 13398–13407.
50 N. A. Malvadkar, M. J. Hancock, K. Sekeroglu, W. J. Dressick and M. C. Demirel, *Nat. Mater.*, 2010, **9**, 1023–1028.
51 S. Daniel, M. K. Chaudhury and J. C. Chen, *Science*, 2001, **291**, 633–636.
52 Q. Wang, X. Yao, H. Liu, D. Quere and L. Jiang, *Proc. Natl. Acad. Sci. U. S. A.*, 2015, **112**, 9247–9252.
53 P. Peruzzo, A. Defina, H. M. Nepf and R. Stocker, *Phys. Rev. Lett.*, 2013, **111**, 164501.
54 J. Jiang, J. Gao, H. Zhang, W. He, J. Zhang, D. Daniel and X. Yao, *Proc. Natl. Acad. Sci. U. S. A.*, 2019, **116**, 2482–2487.
55 M. Cavallaro, Jr., L. Botto, E. P. Lewandowski, M. Wang and K. J. Stebe, *Proc. Natl. Acad. Sci. U. S. A.*, 2011, **108**, 20923–20928.
56 V. Paunov, P. Kralchevsky, N. Denkov and K. Nagayama, *J. Colloid Interface Sci.*, 1993, **157**, 100–112.
57 L. Feng, S. Li, Y. Li, H. Li, L. Zhang, J. Zhai, Y. Song, B. Liu, L. Jiang and D. Zhu, *Adv. Mater.*, 2002, **14**, 1857–1860.
58 A. R. Parker and C. R. Lawrence, *Nature*, 2001, **414**, 33–34.
59 J. Hou, G. Zhou, Y. Wang and D. Guan, *Microporous Mesoporous Mater.*, 2021, **324**, 111260.
60 M. Xia, D. Cai, J. Feng, P. Zhao, J. Li, R. Lv, G. Li, L. Yan, W. Huang, Y. Li, Z. Sui, M. Li, H. Wu, Y. Shen, J. Xiao, D. Wang and Q. Chen, *Adv. Funct. Mater.*, 2023, **33**, 2214813.

61 W. Barthlott and C. Neinhuis, *Planta*, 1997, **202**, 1–8.
62 Z. Guo and W. Liu, *Plant Sci.*, 2007, **172**, 1103–1112.
63 Q. Cheng, M. Li, Y. Zheng, B. Su, S. Wang and L. Jiang, *Soft Matter*, 2011, **7**, 5948–5951.
64 M. Kumar and R. Bhardwaj, *Sci. Rep.*, 2020, **10**, 935.
65 S. Nishimoto and B. Bhushan, *RSC Adv.*, 2013, **3**, 671–690.
66 V. Sharma, H. Ali-Loytty, A. Koivikko, K. Yiannacou, K. Lahtonen and V. Sariola, *Langmuir*, 2021, **37**, 3370–3381.
67 X. Su, D. Hao, P. Li, M. Yang, X. Guo, X. Ai, T. Zhao and L. Jiang, *J. Mater. Chem. A*, 2023, **11**, 7702–7710.
68 J. J. Oladimeji, P. L. Kumar, A. Abe, R. R. Vetukuri and R. Bhattacharjee, *Agronomy*, 2022, **12**, 2094.
69 Y. Y. Yan, N. Gao and W. Barthlott, *Adv. Colloid Interface Sci.*, 2011, **169**, 80–105.
70 V. B. Damodaran and N. S. Murthy, *Biomater. Res.*, 2016, **20**, 1–11.
71 M. K. Chaudhury and G. M. Whitesides, *Science*, 1992, **256**, 1539–1541.
72 X. Yan, B. Ji, L. Feng, X. Wang, D. Yang, K. F. Rabbi, Q. Peng, M. J. Hoque, P. Jin and E. Bello, *ACS Nano*, 2022, **16**, 12910–12921.
73 H. Chen, P. Zhang, L. Zhang, H. Liu, Y. Jiang, D. Zhang, Z. Han and L. Jiang, *Nature*, 2016, **532**, 85–89.
74 J. Ju, Y. Zheng and L. Jiang, *Acc. Chem. Res.*, 2014, **47**, 2342–2352.
75 L. Guo, S. Kumar, M. Yang, G. Tang and Z. Liu, *Nanoscale*, 2022, **14**, 525–533.
76 S. Yi, J. Wang, Z. Chen, B. Liu, L. Ren, L. Liang and L. Jiang, *Adv. Mater. Technol.*, 2019, **4**, 1900727.
77 E. Shanyengana, J. Henschel, M. Seely and R. Sanderson, *Atmos. Res.*, 2002, **64**, 251–259.
78 F. D. Eckardt and R. S. Schemenauer, *Atmos. Environ.*, 1998, **32**, 2595–2599.
79 W. J. Hamilton III and M. K. Seely, *Nature*, 1976, **262**, 284–285.
80 F. Vollrath and D. T. Edmonds, *Nature*, 1989, **340**, 305–307.
81 C. Gehring, D. Williams, S. Cody and R. Parish, *Nature*, 1990, **345**, 528–530.
82 J. M. Gosline, M. E. DeMont and M. W. Denny, *Endeavour*, 1986, **10**, 37–43.
83 Y. Zheng, H. Bai, Z. Huang, X. Tian, F. Q. Nie, Y. Zhao, J. Zhai and L. Jiang, *Nature*, 2010, **463**, 640–643.
84 O. Emile, A. Le Floch and F. Vollrath, *Nature*, 2006, **440**, 621.
85 H. Zhu, Z. Guo and W. Liu, *Chem. Commun.*, 2016, **52**, 3863–3879.
86 A. Almasian, G. Chizari Fard, M. Mirjalili and M. Parvinzadeh Gashti, *J. Ind. Eng. Chem.*, 2018, **62**, 146–155.
87 H. Xu and J. J. Zwiazek, *Front. Plant Sci.*, 2020, **11**, 302.
88 Y. Zhang, C. Zhu, J. Shi, S. Yamanaka and H. Morikawa, *ACS Sustainable Chem. Eng.*, 2022, **10**, 12529–12539.
89 M. R. Islam, G. Tudryn, R. Bucinell, L. Schadler and R. C. Picu, *Sci. Rep.*, 2017, **7**, 13070.
90 F. Ito, S. Komatsubara, N. Shigezawa, H. Morikawa, Y. Murakami, K. Yoshino and S. Yamanaka, *Appl. Phys. Lett.*, 2015, **106**, 133701.
91 H. Sun, Y. Song, B. Zhang, Y. Huan, C. Jiang, H. Liu, T. Bao, S. Yu and H. Wang, *Appl. Phys. A: Mater. Sci. Process.*, 2021, **127**, 461.
92 K. Yin, H. Du, X. Dong, C. Wang, J. A. Duan and J. He, *Nanoscale*, 2017, **9**, 14620–14626.
93 O. Al-Khayat, J. K. Hong, D. M. Beck, A. I. Minett and C. Neto, *ACS Appl. Mater. Interfaces*, 2017, **9**, 13676–13684.
94 S. Wang, M. Liu, Y. Feng, Y. Bu, S. H. Huynh, T. W. Ng, F. Gu, A. Yu and X. Jiang, *J. Mater. Chem. A*, 2017, **5**, 21422–21428.
95 M. Rajaram, X. Heng, M. Oza and C. Luo, *Colloids Surf., A*, 2016, **508**, 218–229.
96 X. Tian, H. Bai, Y. Zheng and L. Jiang, *Adv. Funct. Mater.*, 2011, **21**, 1398–1402.
97 H. Dong, N. Wang, L. Wang, H. Bai, J. Wu, Y. Zheng, Y. Zhao and L. Jiang, *ChemPhysChem*, 2012, **13**, 1153–1156.
98 H. Bai, R. Sun, J. Ju, X. Yao, Y. Zheng and L. Jiang, *Small*, 2011, **7**, 3429–3433.
99 X. Hu, M. Tian, N. Pan, B. Sun, Z. Li, Y. Ma, X. Zhang, S. Zhu, Z. Chen and L. Qu, *Carbon*, 2019, **152**, 106–113.
100 H. Venkatesan, J. Chen, H. Liu, W. Liu and J. Hu, *Adv. Funct. Mater.*, 2020, **30**, 2002437.
101 Y. Chen, L. Wang, Y. Xue, Y. Zheng and L. Jiang, *Soft Matter*, 2012, **8**, 11236–11239.
102 H. Bai, J. Ju, R. Sun, Y. Chen, Y. Zheng and L. Jiang, *Adv. Mater.*, 2011, **23**, 3708–3711.
103 P. Renvoisé, J. W. M. Bush, M. Prakash and D. Quéré, *EPL*, 2009, **87**, 39901.
104 H. Bai, X. Tian, Y. Zheng, J. Ju, Y. Zhao and L. Jiang, *Adv. Mater.*, 2010, **22**, 5521–5525.
105 Y. Chen, D. Li, T. Wang and Y. Zheng, *Sci. Rep.*, 2016, **6**, 19978.
106 L. T. Nguyen, Z. Bai, J. Zhu, C. Gao, H. Luu, B. Zhang and J. Guo, *ACS Sustainable Chem. Eng.*, 2022, **10**, 11176–11190.
107 N. G. Kowalski and J. B. Boreyko, *Soft Matter*, 2022, **18**, 7148–7158.
108 J. H. Lee, Y. J. Lee, H.-Y. Kim, M.-W. Moon and S. J. Kim, *ACS Appl. Mater. Interfaces*, 2022, **14**, 21713–21726.
109 Y. Liu, N. Yang, C. Gao, X. Li, Z. Guo, Y. Hou and Y. Zheng, *ACS Appl. Mater. Interfaces*, 2020, **12**, 28876–28884.
110 H. Park, J. Hwang, T. H. Lee, J. Lee and D. J. Kang, *ACS Appl. Mater. Interfaces*, 2021, **13**, 27575–27585.
111 B. Becher-Nienhaus, G. Liu, R. J. Archer and A. Hozumi, *Langmuir*, 2020, **36**, 7835–7843.
112 H. Liu, Y. Wang, W. Yin, H. Yuan, T. Guo and T. Meng, *J. Mater. Chem. A*, 2022, **10**, 7130–7137.
113 M. O. Aijaz, S. B. Yang, M. R. Karim, M. H. D. Othman and I. A. Alnaser, *Membranes*, 2023, **13**, 32.
114 Y. Y. Song, Y. Liu, H. B. Jiang, S. Y. Li, C. Kaya, T. Stegmaier, Z. W. Han and L. Q. Ren, *Sci. Rep.*, 2017, **7**, 12056.
115 L. Zhong, R. Zhang, J. Li, Z. Guo and H. Zeng, *Langmuir*, 2018, **34**, 15259–15267.
116 M. Gürsoy, M. T. Harris, J. O. Downing, S. N. Barrientos-Palomo, A. Carletto, A. E. Yaprak, M. Karaman and J. P. S. Badyal, *Colloids Surf., A*, 2017, **529**, 195–202.

117 K. C. Park, P. Kim, A. Grinthal, N. He, D. Fox, J. C. Weaver and J. Aizenberg, *Nature*, 2016, **531**, 78–82.
118 H. Bai, T. Zhao, X. Wang, Y. Wu, K. Li, C. Yu, L. Jiang and M. Cao, *J. Mater. Chem. A*, 2020, **8**, 13452–13458.
119 R. Feng, C. Xu, F. Song, F. Wang, X. L. Wang and Y. Z. Wang, *ACS Appl. Mater. Interfaces*, 2020, **12**, 12373–12381.
120 P. Kim, M. J. Kreder, J. Alvarenga and J. Aizenberg, *Nano Lett.*, 2013, **13**, 1793–1799.
121 Y. Chenxi, W. Jian, L. Juan, Z. Haiou, C. Tianqing, G. Zhen, W. Yingguo and B. Bo, *ACS Sustainable Chem. Eng.*, 2023, **11**, 3147–3159.
122 W.-l Zhou, T. Wu, Y. Du, X.-h Zhang, X.-c Chen, J.-b Li, H. Xie and J.-p Qu, *Chem. Eng. J.*, 2023, **453**, 139784.
123 J. Guo, W. Huang, Z. Guo and W. Liu, *Nano Lett.*, 2022, **22**, 3104–3111.
124 J. Zhang, Y. Zhang, J. Yong, X. Hou and F. Chen, *Opt. Laser Technol.*, 2022, **146**, 107593.
125 Y. Zhang, N. Meng, A. A. Babar, X. Wang, J. Yu and B. Ding, *Nano Lett.*, 2021, **21**, 7806–7814.
126 J. Feng, L. Zhong and Z. Guo, *Chem. Eng. J.*, 2020, **388**, 124283.
127 W. Zhou, T. Wu, Y. Du, X. Zhang, X. Chen, J. Li, H. Xie and J. Qu, *Chem. Eng. J.*, 2023, **453**, 139784.
128 X. Wang, W. Zhang, S. Li, Z. Guo and W. Liu, *Chem. Eng. J.*, 2023, **472**, 145042.
129 J. Wu, Z. Yan, Y. Yan, C. Li and J. Dai, *ACS Appl. Mater. Interfaces*, 2022, **14**, 49338–49351.
130 Y. Ding, K. Tu, I. Burgert and T. Keplinger, *J. Mater. Chem. A*, 2020, **8**, 22001–22008.
131 V. Sh Yalishev, N. A. Abbasi, M. Iqbal and A. S. Alnaser, *Langmuir*, 2023, **39**, 1815–1825.
132 W. Zhou, C. Zhou, C. Deng, L. Chen, X. Zeng, Y. Zhang, L. Tan, B. Hu, S. Guo and L. Dong, *Adv. Funct. Mater.*, 2022, **32**, 2113264.
133 J. Tang, L. Peng, D. Chen, J. Xie, M. Chen, J. Wu, X. Hao, W. Cai, F. Zheng and J. Shi, *ACS Appl. Mater. Interfaces*, 2022, **14**, 2202–2210.
134 M. Song, Z. Zhu, J. Qi, Y. Zhou and J. Li, *Environ. Sci.: Nano*, 2023, **10**, 996–1002.
135 F. Bai, J. Wu, G. Gong and L. Guo, *Adv. Sci.*, 2015, **2**, 1500047.
136 X. Ma, M. Cao, C. Teng, H. Li, J. Xiao, K. Liu and L. Jiang, *J. Mater. Chem. A*, 2015, **3**, 15540–15545.
137 Y. Cheng, S. Zhang, S. Liu, J. Huang, Z. Zhang, X. Wang, Z. Yu, S. Li, Z. Chen, Y. Zhao, Y. Lai, X. Qian and C. Xiao, *J. Cleaner Prod.*, 2021, **315**, 127862.
138 Z. Yu, H. Zhang, J. Huang, S. Li, S. Zhang, Y. Cheng, J. Mao, X. Dong, S. Gao, S. Wang, Z. Chen, Y. Jiang and Y. Lai, *J. Mater. Sci. Technol.*, 2021, **61**, 85–92.
139 M. Zhang, Z. Zheng, Y. Zhu, Z. Zhu, T. Si and R. X. Xu, *Chem. Eng. J.*, 2022, **433**, 134495.
140 M. Zhang, S. Wang, Y. Zhu, Z. Zhu, T. Si and R. X. Xu, *Mater. Horiz.*, 2021, **8**, 1756–1768.
141 C. Guo, C. Wang, Q. Huang, Z. Wang, X. Gong and S. Ramakrishna, *Heliyon*, 2022, **8**, e10007.
142 T. Xu, Y. Lin, M. Zhang, W. Shi and Y. Zheng, *ACS Nano*, 2016, **10**, 10681–10688.
143 Z. Yu, S. Li, M. Liu, R. Zhu, M. Yu, X. Dong, Y. Sun and S. Fu, *J. Mater. Chem. A*, 2022, **10**, 304–312.
144 J. Wu, Z. Yan, Y. Yan, C. Li and J. Dai, *ACS Appl. Mater. Interfaces*, 2022, **14**, 49338–49351.
145 J. Wang, S. Yi, Z. Yang, Y. Chen, L. Jiang and C. P. Wong, *ACS Appl. Mater. Interfaces*, 2020, **12**, 21080–21087.
146 Z. Yu, J. Zhang, S. Li, Z. Zhou, Z. Qin, H. Liu, Y. Lai and S. Fu, *Adv. Funct. Mater.*, 2023, **33**, 2210730.
147 H. Xie, Y. Du, W. Zhou, W. Xu, C. Zhang, R. Niu, T. Wu and J. Qu, *Small*, 2023, **19**, 2300915.
148 V.-T. Nguyen, E. Park, N.-A. Nguyen, O. Omelianovych, L. L. Larina, S. S. Hussain and H.-S. Choi, *Appl. Surf. Sci.*, 2023, **615**, 156418.
149 W. S. Wong, M. Li, D. R. Nisbet, V. S. Craig, Z. Wang and A. Tricoli, *Sci. Adv.*, 2016, **2**, e1600417.
150 J. S. Price, *Bound.-Layer Meteorol.*, 1991, **57**, 391–406.
151 M. Zhou, X. He, X. Wu, L. Xiao, Z. Cui, X. Tang, L. Guo, S. Liu, H. Liu and Y. Zhu, *Appl. Mater. Today*, 2020, **21**, 100851.
152 H. Bai, C. Zhang, Z. Long, H. Geng, T. Ba, Y. Fan, C. Yu, K. Li, M. Cao and L. Jiang, *J. Mater. Chem. A*, 2018, **6**, 20966–20972.
153 W.-X. He, X.-W. Wang, Z.-W. Chu, X.-J. Ma, C. Sun and J.-Y. Zhang, *Colloids Surf., A*, 2023, **657**, 130512.
154 H. Chen, T. Ran, K. Zhang, D. Chen, Y. Gan, Z. Wang and L. Jiang, *Glob. Chall.*, 2021, **5**, 2100087.
155 S. Zhang, M. Chi, J. Mo, T. Liu, Y. Liu, Q. Fu, J. Wang, B. Luo, Y. Qin, S. Wang and S. Nie, *Nat. Commun.*, 2022, **13**, 4168.
156 Q. Wang, Y. He, X. Geng, Y. Hou and Y. Zheng, *ACS Appl. Mater. Interfaces*, 2021, **13**, 48292–48300.
157 Y. Su, L. Chen, Y. Jiao, J. Zhang, C. Li, Y. Zhang and Y. Zhang, *ACS Appl. Mater. Interfaces*, 2021, **13**, 26542–26550.
158 Y. Zhang, Y. Jiao, C. Li, C. Chen, J. Li, Y. Hu, D. Wu and J. Chu, *Int. J. Extreme Manuf.*, 2020, **2**, 032002.
159 Y. Guo, Y. Li, G. Zhao, Y. Zhang, G. Pan, H. Yu, M. Zhao, G. Tang and Y. Liu, *Langmuir*, 2023, **39**, 4642–4650.
160 Q. Wang, F. Yang, D. Wu and Z. Guo, *Colloids Surf., A*, 2023, **658**, 130584.
161 Y. Zhang, N. Meng, A. A. Babar, X. Wang, J. Yu and B. Ding, *Nano Lett.*, 2021, **21**, 7806–7814.
162 L. Liu, S. Liu, M. Schelp and X. Chen, *ACS Appl. Mater. Interfaces*, 2021, **13**, 29122–29129.
163 P. Zhu, R. Chen, C. Zhou, Y. Tian and L. Wang, *Chem. Eng. J.*, 2021, **415**, 128944.
164 H. Li, Z. Zhang, Z. Ren, Y. Chen, J. Huang, Z. Lei, X. Qian, Y. Lai and S. Zhang, *Chem. Eng. J.*, 2023, **455**, 140863.
165 Y. Zhang, Y. Cai, J. Shi, H. Morikawa and C. Zhu, *Desalination*, 2022, **540**, 115975.
166 X. Zhang, L. Sun, Y. Wang, F. Bian, Y. Wang and Y. Zhao, *Proc. Natl. Acad. Sci. U. S. A.*, 2019, **116**, 20863–20868.
167 P. Peruzzo, A. Defina, H. M. Nepf and R. Stocker, *Phys. Rev. Lett.*, 2013, **111**, 164501.
168 B. T. Ang, C. H. Yap, W. S. Vincent Lee and J. Xue, *Langmuir*, 2018, **34**, 13409–13415.
169 T. Verho, C. Bower, P. Andrew, S. Franssila, O. Ikkala and R. H. Ras, *Adv. Mater.*, 2011, **23**, 673–678.

170 K. Zhang, H. Chen, T. Ran, L. Zhang, Y. Zhang, D. Chen, Y. Wang, Y. Guo and G. Liu, *ACS Appl. Mater. Interfaces*, 2022, **14**, 33993–34001.
171 Z. Chen, L. Dong, D. Yang and H. Lu, *Adv. Mater.*, 2013, **25**, 5352–5359.
172 Y. Cho, T. S. Shim and S. Yang, *Adv. Mater.*, 2016, **28**, 1433–1439.
173 M. Zhang, L. Ma, Q. Wang, P. Hao and X. Zheng, *Colloids Surf., A*, 2020, **604**, 125291.
174 W. Wu, H. Bai, Y. Yang, G. Li, Z. Chen, C. Tang, H. Yin, L. Lai, J. Liu and S. Xuan, *J. Mater. Chem. A*, 2023, **11**, 8873–8885.
175 Z. Qiu, F. Yu, D. Xu, Z. Wang, J. Huang, S. Wang, Y. Yang, Y. Wang, J. Li and Z. Xiao, *Chem. Eng. J.*, 2023, **455**, 140563.
176 N. Bakhtiari, S. Azizian and B. Jaleh, *J. Colloid Interface Sci.*, 2022, **625**, 383–396.
177 Y. Du, T. Wu, X.-L. Li, W.-L. Zhou, C. Ding, Y.-Q. Yang, J.-G. Wei, X. Lu, H. Xie and J.-P. Qu, *iScience*, 2022, **25**, 105107.
178 X. Wang, S. Handschuh-Wang, Y. Xu, L. Xiang, Z. Zhou, T. Wang and Y. Tang, *Adv. Mater. Interfaces*, 2021, **8**, 2100196.
179 J. Knapczyk-Korczak, D. P. Ura, M. Gajek, M. M. Marzec, K. Berent, A. Bernasik, J. P. Chiverton and U. Stachewicz, *ACS Appl. Mater. Interfaces*, 2019, **12**, 1665–1676.
180 L. Zhang, Y. Wang, Z. Wang, G. Liu, Y. Guo, X. Liu, D. Zhang, L. Jiang and H. Chen, *Appl. Phys. Rev.*, 2022, **9**, 041315.
181 L. Chen, W. Li, Z. Gan, Y. Zhou, M. Chen, D. Cui, H. Ge, P. K. Chan, L. Wang and W.-D. Li, *J. Cleaner Prod.*, 2022, **363**, 132444.
182 J. Hou, G. Zhou, Y. Wang and D. Guan, *Microporous Mesoporous Mater.*, 2021, **324**, 111260.
183 H. Sun, Y. Song, B. Zhang, Y. Huan, C. Jiang, H. Liu, T. Bao, S. Yu and H. Wang, *Appl. Phys. A: Mater. Sci. Process.*, 2021, **127**, 461.

